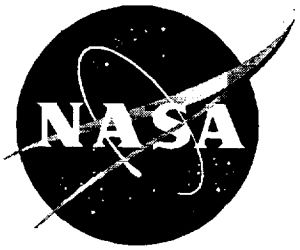

NASA Technical Paper 3461

Natural Frequency of Uniform and Optimized Tetrahedral Truss Platforms

K. Chauncey Wu and Mark S. Lake
Langley Research Center • Hampton, Virginia

National Aeronautics and Space Administration
Langley Research Center • Hampton, Virginia 23681-0001

November 1994

This publication is available from the following sources:

NASA Center for AeroSpace Information
800 Elkridge Landing Road
Linthicum Heights, MD 21090-2934
(301) 621-0390

National Technical Information Service (NTIS)
5285 Port Royal Road
Springfield, VA 22161-2171
(703) 487-4650

Abstract

Qualitative and quantitative estimates for the fundamental frequency of uniform and optimized tetrahedral truss platforms are determined. A semiempirical equation is developed for the frequency of free-free uniform trusses as a function of member material properties, truss dimensions, and parasitic (nonstructural) mass fraction M_p/M_t. Optimized trusses with frequencies approximately two times those of uniform trusses are determined by varying the cross-sectional areas of member groups. Trusses with 3 to 8 rings, no parasitic mass, and member areas up to 25 times the minimum area are optimized. Frequencies computed for ranges of both M_p/M_t and the ratio of maximum area to minimum area are normalized to the frequency of a uniform truss with no parasitic mass. The normalized frequency increases with the number of rings, and both frequency and the ratio of maximum area to minimum area decrease with increasing M_p/M_t. Frequency improvements that are achievable with a limited number of member areas are estimated for a 3-ring truss by using Taguchi methods. Joint stiffness knockdown effects are also considered. Comparison of optimized and baseline uniform truss frequencies indicates that tailoring can significantly increase structural frequency; maximum gains occur for trusses with low values of M_p/M_t. This study examines frequency trends for ranges of structural parameters and may be used as a preliminary design guide.

Introduction

Lattice trusses are a logical choice for large spacecraft structures that require both high stiffness and light weight. While uniform trusses (trusses that are generated by uniform replication of a characteristic cell through space) are inherently efficient structures (ref. 1), higher performance, which may be required for some applications, is attainable with nonuniform trusses. One method used to design nonuniform trusses is to tailor the relative position of the truss nodes in a process called topological design (ref. 2). Since many trusses require a regular pattern of nodes on their surfaces, this technique may not be applicable to some structures and is not investigated here. Another method to improve the performance of a truss with a given nodal arrangement is to tailor the global truss stiffness and mass by varying the truss member cross-sectional areas. This latter approach is used here to improve the performance of a truss platform.

Precise spacecraft pointing requirements for certain science missions, as well as separation of structural and attitude control system frequencies, dictate that the fundamental frequency of the truss structure be maximized. Higher truss frequencies result in lower dynamic amplitudes and faster damping of disturbances. Therefore, spacecraft designers have a particular interest in quantifying the potential improvement in the fundamental frequency of lattice trusses. Because of its simple geometry, the tetrahedral truss is a common truss configuration that is considered for space platforms and is examined in this paper. Although the present study considers only flat truss platforms, the qualitative results should also apply to trusses with a shallow curvature, such as concepts developed for paraboloidal reflectors and aerobrakes supported on doubly curved tetrahedral trusses (refs. 3 and 4).

One common goal in structural optimization is to minimize mass under a given set of frequency and deflection constraints. However, minimum mass is not an appropriate criterion for unconstrained optimization of trusses with no parasitic, or nonstructural, mass. The global truss vibration frequencies are proportional to the ratio of truss stiffness and areal density, which are both proportional to the cross-sectional areas of the truss members. The truss frequencies are therefore independent of the absolute magnitude of the member areas. For example, doubling all member areas doubles both the truss stiffness and areal density, which leaves the global frequency unchanged. Therefore, the minimum mass design of a uniform truss with no parasitic mass is one in which all members have the minimum allowable area. This result does not help to quantify the improvement in truss performance that can result from allowing nonuniform distribution of member cross-sectional areas. The purpose of this study is to address this issue by estimating the increase in

fundamental frequency that is achievable by tailoring the member areas for a nonuniform truss with no parasitic mass, and then considering the effect of parasitic mass on the nonuniform truss frequency.

In the section "Uniform Truss Fundamental Frequency," a closed form, semiempirical expression (eq. (15)) is developed for the fundamental frequency of a free-free uniform truss using laminated plate theory and data from finite element analyses. This equation, which serves as a baseline for the optimized truss analyses, is presented as an explicit function of the truss dimensions, parasitic mass fraction, and truss member material properties. In the section "Near-Optimal Truss Fundamental Frequency," numerical optimization techniques are used to determine nonuniform configurations for trusses with three to eight circumferential rings and no parasitic mass. The term "near optimal" is used to describe these trusses because they represent converged solutions from the optimization process but are not necessarily globally optimal solutions. The changes in frequency due to varying parasitic mass fraction and member area ratio are estimated, and the results are compared with uniform truss frequencies. The section "Influence of Practical Considerations on Near-Optimal Design" addresses two design considerations that affect optimized truss performance. Taguchi design methods are used to quantify the frequency improvement of a 3-ring truss structure with limits on the number of allowable member areas. Truss joint stiffness knockdown effects are also modeled for the 3-ring truss.

This paper provides structural performance data over a wide range of design parameters. As a result, this paper has a broader focus than many previous studies and is intended to serve as a preliminary design guide for spacecraft designers that are considering the use of tetrahedral truss platforms. This study also provides additional insight into the fundamental question of when optimization is warranted. That is, under what conditions does the potential frequency increase justify the additional time, expense, and effort that detail design and fabrication of an optimized structure would require?

Symbols

A	cross-sectional area, m^2
$\overline{A}$	ratio of cross-sectional area to minimum area
a	truss planform area, m^2
D	truss bending stiffness, N-m
d	truss diameter across corners, m
E	truss member elastic modulus, Pa
EA	axial stiffness, N
f	truss fundamental frequency, Hz
$\overline{f}$	ratio of truss frequency to frequency of uniform truss with no parasitic mass
h	truss depth, m
J	joint stiffness knockdown
L	truss member length, m
l	truss strut or joint length, m
M	truss mass, kg
n	number of circumferential truss rings
α, β, κ	empirical coefficients used to compute frequency of uniform truss
δ	correction term for frequency of uniform truss with parasitic mass
P	truss areal density, kg/m^2
ρ	truss member mass density, kg/m^3

Subscripts:

eff	effective value
joint	joint value
max	maximum value
min	minimum value
nom	nominal value
opt	near-optimal truss
opt,0	near-optimal truss with no parasitic mass
p	parasitic mass
strut	strut value
t	total (structural plus parasitic) mass
unif	uniform truss
unif,0	uniform truss with no parasitic mass

Truss Geometry

The tetrahedral truss configuration that is evaluated in this study is assembled from all equal-length truss members. An example of the planar truss platform and repeating cell is shown in figure 1(a). Characteristic dimensions of the truss are the diameter

across corners d and the depth h. The members are shown subdivided into 5 circumferential truss rings ($n = 5$) in figure 1(b) and are shown partitioned into upper surface, core, and lower surface in figure 1(c).

The truss members are assumed to be made up of a strut with joints at each end that attach to the truss nodes for assembly (fig. 2(a)). For the purposes of preliminary analysis, the stiffness of the joints is assumed to be equal to the strut stiffness. Parasitic mass is included in this study to represent the mass of the nodes and joints, as well as other distributed systems that are attached to the truss. An example of a distributed system is the array of hexagonal panels shown in figure 2(b), which may be attached to a truss to form a faceted reflector surface or a heat shield for an aerobrake.

Uniform Truss Fundamental Frequency

In this section, a semiempirical equation (eq. (15)) for the natural frequency of a uniform truss is derived by using laminated plate theory and finite element data. Certain assumptions are made regarding the distribution of parasitic mass to simplify analytical modeling. This equation is written as an explicit function of the truss dimensions, parasitic mass fraction, and member material properties. The accuracy of the equation is evaluated and discussed. Frequencies from this equation provide a baseline for comparison with optimized truss frequencies.

Uniform Truss With No Parasitic Mass

Continuum expressions for the bending stiffness D and areal density P of a uniform tetrahedral truss are derived in reference 5. The truss bending stiffness is derived by assuming that the core members have infinite extensional stiffness and that the upper and lower surfaces may be modeled as isotropic face sheets. These expressions for D and P are

$$D = \frac{\sqrt{3}}{4} E A_{\text{strut}} L \tag{1}$$

and

$$P = 6\sqrt{3}\frac{\rho A_{\text{strut}}}{L} \tag{2}$$

All members are assumed to have the same cross-sectional area A_{strut} and length L and are assumed to be fabricated from a material that has an elastic modulus E and mass density ρ.

The natural frequency of an isotropic plate is (ref. 6)

$$f = \frac{1}{2\pi}\kappa\frac{1}{d^2}\sqrt{\frac{D}{P}} \tag{3}$$

The nondimensional term κ is dependent on the vibration mode number, plate shape, and boundary conditions. Equation (3) has been used to predict truss frequencies of truss platforms where the structural behavior is assumed to approximate that of a thin plate (refs. 7 and 8). Since all the truss platforms evaluated in this study have the same boundary conditions and shape, κ is assumed to be a function of the number of truss rings n. Substitution of equations (1) and (2) into equation (3) gives the equation for the fundamental frequency of a uniform truss with no parasitic mass as

$$f_{\text{unif},0} = \frac{1}{4\pi\sqrt{6}}\kappa\frac{L}{d^2}\sqrt{\frac{E}{\rho}} \tag{4}$$

As explained previously, the uniform truss frequency is not dependent on the member area A_{strut}, since both D and P are proportional to A_{strut}. The relationship between the truss depth h and member length is

$$L = \sqrt{\frac{3}{2}}h \tag{5}$$

Substitution of equation (5) into equation (4) gives

$$f_{\text{unif},0} = \frac{1}{8\pi}\kappa\left(\frac{d}{h}\right)^{-1}\frac{1}{d}\sqrt{\frac{E}{\rho}} \tag{6}$$

The relationship between the ratio of truss diameter to depth d/h and n is

$$\frac{d}{h} = \sqrt{\frac{3}{2}}(2n+1) \tag{7}$$

Substitution of equation (7) for d/h in equation (6) results in

$$f_{\text{unif},0} = \frac{1}{8\pi}\sqrt{\frac{2}{3}}\kappa(2n+1)^{-1}\frac{1}{d}\sqrt{\frac{E}{\rho}} \tag{8}$$

Incorporation of all constants (except the conversion factor of 2π rad/cycle) and $(2n+1)^{-1}$ into κ allows equation (8) to be rewritten as

$$f_{\text{unif},0} = \frac{1}{2\pi}\kappa\frac{1}{d}\sqrt{\frac{E}{\rho}} \tag{9}$$

The frequency is now a function of the truss dimensions (d and n) and the member elastic modulus-to-density ratio E/ρ. The conversion factor of 2π rad/cycle is kept separate to ensure that κ is nondimensional.

The coefficient κ is empirically determined from finite element analyses of free-free uniform trusses

with no parasitic mass and 1 to 10 rings. A linear-analysis model is built from pinned-end axial-force elements by using a commercial finite element code (ref. 9). The truss members are 2 m in length, with an elastic modulus of 1.23×10^{11} Pa and a mass density of 1348 kg/m^3 (nominal properties for a high-performance graphite-epoxy material). A vibrational analysis is performed to determine the lowest flexible-body frequency of each truss. Empirical values of κ are computed from the finite element data in appendix A and are listed in table 1. The mode shape for the truss fundamental frequency, shown for a 5-ring truss in figure 3, is an asymmetric, anticlastic bending of the truss.

Uniform Truss With Parasitic Mass

Parasitic mass is assumed to represent node and joint mass, reflector or aerobrake panels, or other nonstructural distributed systems such as thermal insulation. The only effect of parasitic mass is to lower the truss frequency, since inclusion of parasitic mass contributes nothing to the structural stiffness. If the total (structural plus parasitic) mass is defined as M_t, the frequency of a uniform truss with parasitic mass is, from equation (3),

$$f = \frac{1}{2\pi}\kappa\frac{1}{d^2}\sqrt{\frac{aD}{M_t}} \tag{10}$$

since the areal density P is equal to M/a, where a is the truss planform area. Similarly, the frequency of a uniform truss with no parasitic mass is

$$f = \frac{1}{2\pi}\kappa\frac{1}{d^2}\sqrt{\frac{aD}{M_t - M_p}} \tag{11}$$

where M_p is the parasitic mass. If parasitic mass is distributed around a uniform truss in identical proportions to the structural mass distribution, the constants in equations (10) and (11) are equal. The normalized frequency of a uniform truss with a proportional parasitic mass distribution $\overline{f}$ may be written as the ratio of equation (10) to equation (11), which simplifies to

$$\overline{f} = \sqrt{1 - \frac{M_p}{M_t}} \tag{12}$$

where the parasitic mass fraction M_p/M_t is the ratio of parasitic mass to total mass. The normalized frequency $\overline{f}$ decreases as M_p/M_t increases, and as M_p/M_t approaches the limiting value of 1, $\overline{f}$ approaches 0 because almost all the mass is parasitic. Since most truss structures do not have parasitic mass that is distributed proportionally to structural mass, equation (12) is only an approximation of the true behavior of most trusses.

By subtracting a correction term δ from equation (12), which accounts for the nonproportional distribution of parasitic mass, the normalized frequency of a uniform truss with parasitic mass is defined as

$$\overline{f}_{\text{unif}} \equiv \frac{f_{\text{unif}}}{f_{\text{unif},0}} = \sqrt{1 - \frac{M_p}{M_t}} - \delta \tag{13}$$

where f_{unif} is the frequency of a uniform truss with a nonproportional parasitic mass distribution. The analyses in appendix B show that many types of parasitic mass are accurately represented by an assumed distribution in which the same mass is placed at each truss interior node on both the upper and lower surfaces, and two-thirds of this mass is placed at each perimeter node (in the outermost truss ring). This nonproportional distribution of parasitic mass is used to quantify the reduction in uniform truss frequency due to parasitic mass. Rigid point masses are assigned to each truss node according to the nonproportional distribution just described. Fundamental frequencies are then computed with finite element analyses for uniform trusses with from 1 to 10 rings as M_p/M_t is varied from 0 to 0.95. These frequencies are normalized by $f_{\text{unif},0}$ and are plotted against M_p/M_t in figure 4 for 1- to 5-ring trusses (the data for 6- to 10-ring trusses are omitted for clarity). The normalized frequency of a uniform truss with a proportional parasitic mass distribution (eq. (12)) is also shown as the uppermost curve in figure 4.

The difference between the normalized frequencies with proportionally distributed parasitic mass and nonproportionally distributed parasitic mass is the correction term δ in equation (13). The term δ is computed for each of the 10 trusses and is shown for 1- to 5-ring trusses in figure 5. Note that δ approaches 0 as n increases. This trend indicates that the difference between the proportionally distributed parasitic mass and the nonproportionally distributed parasitic mass has little effect on the fundamental frequency of large trusses, whereas the difference in parasitic mass distribution has a significant effect for small trusses. A function[1] that equals 0 when

[1]The authors are grateful to W. B. Fichter for the form of δ in equation (14).

$M_p/M_t = 0$ or 1 is chosen to provide a closed-form approximation to δ. The function selected for δ is

$$\delta = \alpha\left(1 - \frac{M_p}{M_t}\right)\left[1 - \left(1 - \frac{M_p}{M_t}\right)^{\beta}\right] \qquad (14)$$

Empirical values of α and β are computed from finite element data in appendix A and are shown in table 1.

Equations (9), (13), and (14) are combined into a closed-form equation for the fundamental frequency of a free-free uniform tetrahedral truss,

$$f_{\text{unif}} = \left[\frac{1}{2\pi}\kappa\frac{1}{d}\sqrt{\frac{E}{\rho}}\right]\left\{\sqrt{1 - \frac{M_p}{M_t}} - \alpha\left(1 - \frac{M_p}{M_t}\right) \times \left[1 - \left(1 - \frac{M_p}{M_t}\right)^{\beta}\right]\right\} \qquad (15)$$

and empirical values of κ, β, and α are shown in table 1. Equation (15) is applicable to trusses with integer values of n from 2 to 10. In this study, uniform truss frequencies computed with equation (15) are used to provide baseline values for comparison with fundamental frequencies of near-optimal trusses.

Verification

Accuracy of uniform truss frequencies predicted with equation (15) is determined for 3- and 5-ring trusses with various parasitic-mass distributions. Finite element models of these trusses are generated with parasitic mass representing truss nodes and joints and reflector or heat-shield panels. (See fig. 2.) Each truss node is represented by a 0.39-kg point mass, and each truss joint is represented by a 0.21-kg point mass. Each panel is represented by three 4.08-kg point masses; these point masses are located at the upper surface nodes where the panels are attached. Two parasitic mass cases are evaluated. The first case includes the node, joint, and panel parasitic mass, and the second case includes only the node and joint mass. In both cases, the truss parasitic mass fraction is varied by uniformly varying the member cross-sectional area from 6.45×10^{-5} to 3.23×10^{-4} m^2.

Normalized frequencies predicted with equation (15) and with data from finite element analyses are plotted in figures 6(a) and (b) for 3- and 5-ring trusses. These plots show that equation (15) accurately predicts the frequency of trusses with only node and joint mass, but slightly overestimates the frequency of trusses with nodes, joints, and panels. Despite the simplified parasitic mass distribution used to obtain equation (15), all predicted frequencies are within 3 percent of the corresponding values from finite element analyses. These results indicate that equation (15) is sufficiently accurate for preliminary design of tetrahedral truss platforms.

Since equation (15) is presented as an explicit function of n, d, E/ρ, and M_p/M_t, it is very useful for parametric analyses of uniform trusses. For example, if the truss dimensions (n and d) are known for a given application, the parameters κ, β, and α are found in table 1. Equation (15) is then used to describe curves (similar to fig. 6) that are used as a design plot to determine the maximum parasitic mass fraction for a given fundamental frequency or to determine the variation of truss frequency with member E/ρ.

Near-Optimal Truss Fundamental Frequency

In this section, numerical optimization techniques are used to determine member cross-sectional area tailoring schemes that increase the fundamental frequencies of trusses with 3 to 8 rings. Initially, trusses with no parasitic mass are evaluated. Also, the ratio of the maximum cross-sectional area to the minimum area of the truss members is constrained to be no greater than 25. From these analytical results, estimates are made of the variation in truss frequencies due to the reduction of the ratio of the maximum area to the minimum area from 25 to 5, 10, 15, and 20. Finally, the reduction in optimized truss frequency due to parasitic mass is evaluated.

Near-Optimal Truss With No Parasitic Mass

The objective of these analyses is to determine truss member cross-sectional areas of near-optimal trusses, which have the highest attainable fundamental frequency. A numerical optimization routine, contained in the finite element code of reference 9, is used to maximize the lowest flexible-body frequency of free-free trusses with 3 to 8 rings and no parasitic mass. To reduce the number of design variables, the truss members are partitioned into groups that each contain a small number of members. The members within each group are required to have the same cross-sectional area, but the areas are allowed to vary between groups. The subdivision scheme partitions each ring of the truss into upper surface, core, and lower surface member groups; this scheme results in a total number of member groups that is equal to 3 times the number of rings. Truss member group numbers are assigned based on the ring number n and the relative position of the group in the truss. In

truss ring n, the upper surface member group number is $3n-2$, the core member group number is $3n-1$, and the lower surface group number is $3n$. The 9 member groups for a 3-ring truss are illustrated in figure 7.

The truss member group cross-sectional areas are chosen as the design variables. Constraints imposed on the design variables represent practical upper and lower bounds on the member areas. The minimum member area A_{min} is 6.45×10^{-5} m^2. In an actual application, this value would be determined from considerations such as local member frequency or buckling load, strut minimum-gage fabrication constraints, or member handling requirements. The normalized member area $\overline{A}$ is as follows:

$$\overline{A} \equiv \frac{A_{\text{strut}}}{A_{\text{min}}} \tag{16}$$

where A_{strut} is the strut cross-sectional area. The maximum normalized member area is calculated as follows:

$$\overline{A}_{\text{max}} \equiv \frac{A_{\text{max}}}{A_{\text{min}}} \tag{17}$$

where A_{max} is the maximum member area. In this portion of the study, $A_{\text{max}} = 1.61 \times 10^{-3}$ m^2 and $\overline{A}_{\text{max}} = 25$; $\overline{A}_{\text{max}}$ represents the maximum variation in the truss member areas, not the normalized areas of the individual truss member groups.

The normalized frequency for a near-optimal truss with no parasitic mass is defined as

$$\overline{f}_{\text{opt},0} \equiv \frac{f_{\text{opt},0}}{f_{\text{unif},0}} \tag{18}$$

where $f_{\text{opt},0}$ is the fundamental frequency of an optimized truss with no parasitic mass. Normalized member areas, determined from finite element and numerical optimization analyses, are listed in table 2 with corresponding normalized frequencies for near-optimal trusses with 3 to 8 rings and $\overline{A}_{\text{max}} = 25$. These near-optimal truss configurations all show similar trends. Member groups in the truss interior have large cross-sectional areas, because these members have the lowest mass moment of inertia and the largest impact on the truss bending stiffness. Areas of member groups towards the outermost truss ring are all at or near minimum values, because these members have the highest inertia and contribute the least to the structural stiffness. In each case, the normalized frequency of a near-optimal truss is about two times that of a uniform truss with equal n, which shows that optimization can have a significant effect on structural performance. Also, the normalized near-optimal frequencies increase slightly as n increases, because the number of member groups, and thus the number of design variables, both increase.

To evaluate the sensitivity of truss frequencies to variation in member cross-sectional area ratio, normalized member areas of the near-optimal truss configurations (computed for $\overline{A}_{\text{max}} = 25$) in table 2 are linearly scaled to $\overline{A}_{\text{max}} = 5$, 10, 15, and 20 as follows:

$$\overline{A}|_{\overline{A}_{\text{max}}} = \frac{\overline{A}_{\text{max}} - 1}{24}\left(\overline{A}|_{\overline{A}_{\text{max}}=25} - 1\right) + 1 \tag{19}$$

The resulting truss configurations are then analyzed with finite element methods to determine their fundamental frequencies. A surface plot of the normalized frequencies is shown in figure 8 for ranges of both $\overline{A}_{\text{max}}$ and n. Also shown are data for a uniform truss, with $\overline{A}_{\text{max}}$ and normalized frequency both equal to 1. These analyses show that the near-optimal truss frequency decreases significantly with decreasing $\overline{A}_{\text{max}}$. Although larger member area ratios are beyond the scope of the present study, the truss frequencies could probably be increased beyond the levels presented here if the area ratios were allowed to be larger than 25. However, area ratios over 25 are probably impractical for most applications.

Near-Optimal Truss With Parasitic Mass

To estimate the reduction in near-optimal truss frequencies caused by parasitic mass, the truss configurations presented in table 2 and computed from equation (19) are analyzed with parasitic mass at the truss nodes. Fundamental frequencies are computed with finite element analyses for trusses with discrete values of M_p/M_t from 0 to 0.95. The nonproportional parasitic mass distribution developed in appendix B for uniform trusses is again used to determine the parasitic mass assigned to each truss node. The normalized frequency for a near-optimal truss with parasitic mass is

$$\overline{f}_{\text{opt}} \equiv \frac{f_{\text{opt}}}{f_{\text{unif},0}} \tag{20}$$

where f_{opt} is the frequency of a near-optimal truss with parasitic mass.

The results of these analyses are shown in figure 9 for a 3-ring truss. Each curve in the figure represents the performance of an optimized 3-ring truss with a different member area ratio. The near-optimal truss is identified as the truss that has the highest frequency at any given value of M_p/M_t. The area ratio of the near-optimal configuration decreases as M_p/M_t increases. Furthermore, the curves in figure 9 suggest that area ratios greater than 25 would

only improve truss performance if M_p/M_t were less than 0.15. Since trusses with such low parasitic mass fractions are unlikely in most practical applications, allowing area ratios over 25 is probably not necessary.

The locus of normalized frequencies for the near-optimal 3-ring truss is presented in figure 10 along with the uniform truss frequencies computed from equation (15). The frequency improvement from structural optimization varies from over 80 percent for $M_p/M_t = 0$ to about 5 percent for $M_p/M_t = 0.95$. These results indicate that optimization has a significant impact on the fundamental frequency when M_p/M_t is very low. For a truss with a high value of M_p/M_t, optimization has a much smaller effect on structural performance. Similar behavior is shown in figure 11 for near-optimal trusses with 3 to 8 rings, although the magnitude of the normalized frequency does increase slightly with an increasing number of rings.

Verification

Numerical optimization analyses are performed for a 3-ring truss with fixed values of $M_p/M_t = 0.25$, 0.50, and 0.75 to evaluate the accuracy of the near-optimal frequencies in figure 10. Two parasitic-mass cases (node, joint, and panel parasitic mass, and only node and joint mass) are used for these analyses. Frequencies from the numerical optimization and finite element analyses are shown in figure 12 and are compared with the near-optimal truss frequencies from figure 10. The optimized truss frequencies differ by no more than 5 percent from the corresponding computed values. The maximum normalized member areas are computed from equation (16) for the four optimized truss configurations in figure 12. These values of $\overline{A}_{\max}$, shown in table 3, decrease as M_p/M_t increases; this decrease reflects the trends in figure 9, where the area ratio of the truss with the highest frequency decreases with increasing M_p/M_t. Thus, these analyses confirm that the frequency estimates presented in figures 9 to 11 accurately predict the behavior of near-optimal trusses.

Influence of Practical Considerations on Near-Optimal Design

Two practical considerations for truss design that reduce performance from previously computed near-optimal levels are examined in this section. The reductions in frequency due to limits on the number of member cross-sectional areas and joint stiffness knockdown are determined for a 3-ring truss with $\overline{A}_{\max} = 5$. Taguchi design methods are used to evaluate the frequency improvement achievable with a limited number of member areas. These configurations are then analyzed to quantify the effect of joint stiffness knockdown on truss frequency.

Taguchi Design Methods

Taguchi methods (ref. 10) have been successfully applied to design optimization of systems and processes in the automotive and consumer electronics fields and have recently been used for design of aerospace vehicles (ref. 11). The main advantage of using Taguchi methods over other optimization techniques is their simplicity, since Taguchi methods can be implemented with minimal effort with existing analysis tools. Also, unlike most numerical optimization routines, the near-optimal design predicted by this technique is insensitive to the configuration selected as a starting point. The main disadvantage of Taguchi methods is that the solution generated by the analysis is not guaranteed to be *the* global optimum. Also, every combination of design variables is assumed to be feasible, which means that additional constraints cannot be imposed during the optimization process. One potential limitation of Taguchi methods is that the design variables are forced to have discrete values; these values divide the design space into a matrix of discrete configurations. However, for many design applications, practical considerations naturally restrict design variables to discrete or binary values; in these cases, Taguchi methods are most appropriate for design optimization.

Limited Number of Member Areas

The near-optimal truss member group areas calculated in the numerical optimization analyses are only constrained by upper and lower bounds on the member area. Thus, members could have any value between these limits, and the number of different member areas is less than or equal to the number of member groups. However, selection of member cross-sectional areas and the number of different areas are probably limited by manufacturing and logistical considerations. For example, the cross-sectional areas of composite truss members of a given diameter are constrained to discrete values by the layup of the composite material. Such restrictions on the member areas are likely to reduce the maximum performance that is attainable through optimization.

The magnitude of the reduction in frequency is evaluated for a 3-ring truss by restricting each normalized member group area $\overline{A}$ to integer values from 1 to 5. Since there are 9 truss member groups, there are 1.95×10^6 (5^9) possible combinations of design variables. However, a near-optimal configuration can be determined with only 54 separate finite element

analyses with a two-iteration Taguchi method. For the first iteration, each member group has a cross-sectional area of 1, 3, or 5. For the second iteration, groups where $\overline{A} = 1$ from the first iteration are allowed to be 1, 2, or 3. Similarly, groups in which $\overline{A} = 3$ are allowed to be 2, 3, or 4, and groups in which $\overline{A} = 5$ are allowed to be 3, 4, or 5.

Truss configurations from the Taguchi analyses are presented in the form $\overline{A}$ = (123 456 789), where each number in parentheses is the normalized cross-sectional area of member groups 1 to 9 in a 3-ring truss (shown in fig. 7). After the first iteration, the normalized areas for the near-optimal configuration of a 3-ring truss with no parasitic mass are $\overline{A}$ = (555 315 113) with a normalized frequency of 1.25. After the second iteration, the near-optimal configuration has $\overline{A}$ = (555 435 122) with a normalized frequency of 1.32. The member groups in the case with no parasitic mass show a wide range of cross-sectional areas; stiffer members are concentrated in ring 1 and in the upper and lower surface members of ring 2. Members with smaller areas are located in the core of ring 2 and in all levels of ring 3. This two-iteration process is repeated for two parasitic-mass cases; node and joint mass, and node, joint, and panel mass. Predicted truss configurations from the Taguchi analyses are shown in table 4 with normalized frequencies and parasitic mass fractions computed from finite element analyses. The distribution of truss member areas described here for the case without parasitic mass is similar to trends observed for the case with node and joint mass. However, almost all the members in the truss with node, joint, and panel mass have the maximum possible cross-sectional area. These analyses suggest that, as the truss parasitic mass fraction increases, the near-optimal truss configuration approaches a uniform truss in which all members have the same cross-sectional area.

Normalized frequencies for the six trusses described in this section are plotted in figure 13; the estimated near-optimal truss frequency curve ($\overline{A}_{\max} = 5$) is from previous finite element analyses (fig. 9), and the uniform truss frequency curve is from equation (15). As expected, these two curves are bounding values for the Taguchi analysis data. The estimated near-optimal frequency curve is computed by allowing each of the 9 truss member groups to have any cross-sectional area between the upper and lower bounds. In contrast, the data points in figure 13 represent near-optimal frequencies that may be obtained with only three or five different member areas constrained to integer multiples of the minimum area. Thus, a fairly substantial performance increase can be achieved for the 3-ring truss through optimization with a limited number of member cross-sectional areas. In fact, over 60 percent of the maximum frequency improvement over a uniform truss can be attained by allowing each member group to have one of only three different areas during optimization.

Joint Stiffness Knockdown

Another consideration in design and analysis of trusses is that the effective axial stiffness of the truss member depends on the axial stiffness of the structural joints and the axial stiffness of the strut itself. Since the strut axial stiffness is typically higher than the joint axial stiffness, the effective axial stiffness of the truss member (two joints and a strut) is lower than the axial stiffness of the strut alone. The joint stiffness knockdown (ref. 12) is

$$J = 1 - \frac{EA_{\text{eff}}}{EA_{\text{strut}}} \tag{21}$$

where EA_{strut} is the strut axial stiffness and EA_{eff} is the effective axial stiffness of the truss member as follows:

$$EA_{\text{eff}} = \frac{l_{\text{strut}} + 2l_{\text{joint}}}{(l_{\text{strut}}/EA_{\text{strut}}) + (2l_{\text{joint}}/EA_{\text{joint}})} \tag{22}$$

where l_{strut} and l_{joint} are the strut and joint lengths.

Since the joint stiffness knockdown is the same for each member in a uniform truss, the frequency reduction for a uniform truss is

$$\frac{f_{\text{nom}} - f}{f_{\text{nom}}} = 1 - \sqrt{1 - J} \tag{23}$$

where f_{nom} is the uniform truss frequency with no joint stiffness knockdown. However, the joint stiffness knockdown is different for each different member cross-sectional area in optimized trusses, and a closed-form solution is not available to determine the frequency reduction. To estimate the effect of joint stiffness knockdown on the performance of nonuniform, near-optimal trusses, the 3-ring truss configurations computed in the previous section are reanalyzed to determine the frequency reduction due to joint stiffness knockdown. Based on the assumptions that $l_{\text{strut}} = 5L/6$, $2l_{\text{joint}} = L/6$, the strut and joints are made of materials with equal moduli, and $A_{\text{joint}} = A_{\min}$, the joint stiffness knockdown is

$$J = \frac{\overline{A} - 1}{\overline{A} + 5} \tag{24}$$

where $\overline{A}$ is the normalized strut area defined in equation (16). This joint stiffness knockdown from equation (30) is plotted against $\overline{A}$ in figure 14 and varies from 0 for $\overline{A} = 1$ to 0.40 for $\overline{A} = 5$. Normalized frequencies for the near-optimal truss configurations that include the joint stiffness knockdown are shown in table 4 with corresponding percentage reductions in frequency from the previous analyses without joint stiffness knockdown.

About 45 percent of the members in the two trusses with no parasitic mass have the maximum cross-sectional area, and consequently, the maximum joint stiffness knockdown of 0.40. Frequency reductions of 12 to 17 percent due to joint stiffness knockdown are observed for these trusses. Roughly 60 percent of the members in trusses that are modeled with node and joint mass have the maximum joint stiffness knockdown, and both trusses have frequency reductions of about 19 percent. Almost 90 percent of the members in the trusses with node, joint, and panel mass have the maximum joint stiffness knockdown. These trusses have the largest frequency reductions—about 20 percent. Frequency reductions, computed from equation (23) with $J = 0.40$ approach a limiting value of 22.54 percent.

Concluding Remarks

Qualitative and quantitative trends for uniform and near-optimal tetrahedral truss platform frequencies are presented and discussed. A closed-form semiempirical equation is developed for the fundamental free-free vibration frequency of a uniform tetrahedral truss platform over a range of truss sizes and parasitic mass fractions. This equation may be used by spacecraft designers to accurately and efficiently predict the fundamental frequency of large planar trusses without the time and expense of computational methods. Since this equation is derived as an explicit function of the design variables, it is very useful for parametric analyses of uniform trusses and, in this study, provides a baseline for comparison with truss platforms that have been tailored to maximize the natural frequency.

Numerical optimization techniques are used to determine member area distributions that improve the fundamental frequency of trusses over a wide range of structural parameters. Fundamental frequencies that are about two times the uniform truss frequencies are achievable through optimization of trusses with no parasitic mass and a set of truss member groups equal to 3 times the number of truss rings. As the parasitic mass fraction increases, both the normalized frequency and area ratio of the near-optimal truss configuration decrease; the percent increase in performance achievable through member area optimization also decreases. However, a substantial increase in truss frequency can be realized through optimization with a limited number of different cross-sectional areas for each member group. Analyses with Taguchi design methods suggest that, for a 3-ring truss, over 60 percent of the maximum frequency improvement can be achieved by optimizing with only three different cross-sectional areas.

These analyses show that structural optimization is much more beneficial for trusses with small amounts of parasitic mass. Thus, as the structure becomes more efficient in one sense (with a high parasitic mass fraction), optimization has less of an impact on the structural performance. On the other hand, optimization of an inefficient structure (with a low parasitic mass fraction) can yield significant increases in the fundamental frequency. Although trusses are inherently efficient structures, some consideration should always be given to using optimized configurations to obtain the maximum possible performance on orbit, and any potential increases in performance must always be weighed against increases in complexity, mass, and cost of the structure.

NASA Langley Research Center
Hampton, VA 23681-0001
September 28, 1994

Appendix A

Determination of Empirical Coefficients κ, β, and α

Empirical values for κ, β, and α are used in the closed-form equation for the fundamental frequency of free-free uniform trusses with 1 to 10 rings. These empirical values are computed from finite element data in this appendix. Closed-form equations are also generated for κ, β, and α as functions of n to facilitate computer coding of equation (15).

Determination of κ

To determine empirical values for κ, equation (9) is rearranged to solve for κ, giving

$$\kappa = 2\pi f_{\text{unif},0} d \sqrt{\frac{\rho}{E}} \tag{A1}$$

Equation (A1) is used to compute κ for each truss with the corresponding values of d and $f_{\text{unif},0}$ (table 5) from the finite element analyses described previously. Values of κ are shown in table 5 and are plotted against n in figure 15. Since κ is asymptotic for large values of n, a curve-fit is constructed that consists of n raised to negative integer powers. A computational mathematics program (ref. 13) is used to compute coefficients for the curve-fit. The best-fit equation for κ (defined as having a root-mean-square error less than 0.50 percent with the fewest number of terms) is

$$\kappa = -0.0181 + 2.9778n^{-1} - 4.9461n^{-2} + 4.8929n^{-3} - 2.3455n^{-4} \tag{A2}$$

The curve generated from equation (A2) is plotted in figure 15 for comparison with the tabulated data. Although n is continuous in equation (A2), only integer values of n from 1 to 10 are used in this study.

Determination of β and α

To determine empirical values for β and α, $\delta_{\max}$ and associated values of M_p/M_t, shown in table 5, are estimated from the finite element data for δ versus M_p/M_t (fig. 5). Equation (14) is differentiated with respect to M_p/M_t to derive analytical expressions for $\delta_{\max}$ and the associated M_p/M_t as functions of β and α. These analytical expressions are

$$\frac{M_p}{M_t}\Big|_{\delta=\delta_{\max}} = 1 - (1+\beta)^{-1/\beta} \tag{A3}$$

$$\delta_{\max} = \frac{\alpha\beta}{(1+\beta)^{1+1/\beta}} \tag{A4}$$

A numerical value of β is computed from an iterative solution of equation (A3), and α is then computed directly from equation (A4). These computed values of β and α (table 5) force equation (14) to have the same values of $\delta_{\max}$ and associated M_p/M_t as the data plotted in figure 5. Computed values for β and α from these analyses are also plotted against n in figures 16 and 17.

Curve-fits are made to the computed values in table 5 to determine closed-form equations for β and α as functions of n. Since β is asymptotic for large values of n, a curve-fit for β, consisting of n raised to negative integer powers, is constructed as

$$\beta = -0.2024 - 0.0656n^{-1} + 1.3163n^{-2} - 2.0915n^{-3} + 1.2318n^{-4} \tag{A5}$$

The curve for β generated by equation (A5) is also plotted in figure 16 with the tabulated data. As with equation (A2), equation (A5) is only valid for integer values of n from 1 to 10.

Between $n = 1$ and 2, (fig. 16), $\beta = 0$. From equation (A4), α is indeterminate when $\beta = 0$. Thus, the plot of α versus n has a vertical asymptote between $n = 1$ and 2, which means the curve for α is discontinuous at this point. This observation is verified by the data in figure 17, which show that, in contrast to the positive value of α at $n = 1$, α takes on large negative values as n approaches the asymptote from above. To simplify formulation of an equation for α, the data point at $n = 1$ is omitted and a curve-fit is made to the remaining 9 data points. This equation for α, which is asymptotic for large values of n, is

$$\alpha = -0.0050 + 0.3591n^{-1} - 7.8039n^{-2} + 12.7195n^{-3} - 18.8335n^{-4} \tag{A6}$$

The curve for α that is predicted by equation (A6) is shown in figure 17 with the data from table 5. Equation (A6) is only valid for values of integer n from 2 to 10.

Appendix B

Selection of Approximate Parasitic Mass Distribution

Parasitic mass represents various nonstructural systems and hardware, such as nodes, joints, and reflector or aerobrake panels. Parasitic mass does not contribute to the structural stiffness and only lowers the truss natural frequency. The manner in which parasitic mass is distributed among the truss nodes affects the truss frequency by changing the transverse and rotary inertia of the structure. Although most common types of parasitic mass have near-uniform distributions through the structure, minor differences in their distributions must be modeled accurately if analysis errors are to be minimized. However, for parametric analyses in support of preliminary design, sufficient accuracy can be achieved by lumping all near-uniform parasitic mass together and modeling them with a single approximate mass distribution. In this appendix, a mass distribution that provides a reasonable approximation to the actual distribution of node, joint, and panel mass is described.

Nodes and Joints

Although truss nodes are load-carrying components, their designs are typically driven by truss geometric requirements rather than structural efficiency requirements. Thus, most of the truss node mass is considered to be parasitic. Since each node is assumed to have the same mass, the parasitic mass of the truss nodes is uniformly distributed around the truss.

Since the truss joints incorporate mechanisms that are relatively massive, most of the truss joint mass is also considered to be parasitic. The distribution of joint parasitic mass is slightly nonuniform. Because each truss interior node has 9 attached truss members, the mass of 9 joints is associated with each truss interior node. Each truss perimeter node (on the outermost ring) has 4 to 7 attached members; the average mass of the joints at perimeter nodes is as follows:

$$\text{Average joint mass at perimeter node} = \frac{75n}{12n+3}\,(\text{Joint mass}) \quad \text{(B1)}$$

where n is the number of rings in the truss. Dividing equation (B1) by the mass of nine joints at each interior node yields the following ratio for the average joint mass at a perimeter node to the average joint mass at an interior node as a function of n (joint masses cancel):

$$\frac{\text{Average joint mass at perimeter node}}{\text{Average joint mass at interior node}} = \frac{25n}{36n+9} \quad \text{(B2)}$$

The ratio in equation (B2) asymptotically approaches 25/36 for large values of n and is plotted as a function of n in figure 18.

Panels

As with the joint mass, the panel mass has a slightly nonuniform distribution. Each panel is attached to three nodes on the truss upper surface. Thus, one-third of the panel mass is located at each attachment point. Since three panels are attached to each interior node on the upper surface of the truss, the total mass concentrated at each interior upper surface node is equal to the mass of one panel. However, each perimeter node has either one or two attached panels. An average value for the panel mass associated with each perimeter node can be calculated by multiplying the total number of perimeter panel attachments by one-third of the panel mass and dividing the result by the total number of perimeter upper surface nodes. The total number of perimeter panel attachments is $9n+3$, and the total number of perimeter upper surface nodes is $6n+3$. Thus,

$$\text{Average upper surface panel mass at perimeter node} = \frac{9n+3}{6n+3} \times \left(\frac{\text{Panel mass}}{3}\right) \quad \text{(B3)}$$

Since each interior upper surface node has the mass of one panel concentrated at it, the ratio of the average panel mass at perimeter upper surface nodes to panel mass at interior upper surface nodes is as follows: (panel masses cancel)

$$\frac{\text{Average upper surface panel mass at perimeter node}}{\text{Upper surface panel mass at interior node}} = \frac{3n+1}{6n+3} \quad \text{(B4)}$$

Equation (B4) approaches 3/6 for large values of n and is plotted as a function of n in figure 18.

Figure 18 shows significant differences between the ratios of perimeter-node parasitic mass to interior-node parasitic mass for the three types of parasitic mass considered here. Also, the panel mass is located at only the upper surface nodes, while the node mass and joint mass are distributed to all nodes. Nevertheless, a single distribution may be selected that adequately represents the three types of parasitic mass for preliminary analysis of truss vibration frequencies. Since the fundamental mode of a tetrahedral truss platform is a plate-like mode, rotary inertia effects should be small. Therefore, little

error should be introduced if the panel mass is distributed to both upper and lower surface nodes, as with the node and joint mass. With this simplification, the only parameter that differs in the distribution of the three types of parasitic mass is the ratio of perimeter-node mass to interior-node mass. A compromise value for this ratio is selected based on the finite element analysis in the next paragraph.

Fundamental frequencies are computed for uniform 3-ring trusses with node (0.39 kg each), joint (0.21 kg each), and panel (12.25 kg each) masses added in their exact distributions to the truss nodes. These data are generated for configurations with and without panels on the upper surface, and the resulting data are plotted in figure 19. Different values of parasitic mass fraction are achieved in these analyses by uniformly changing the cross-sectional area of all truss members while holding the parasitic mass constant. Also shown in the figure are three curves that are generated from finite element analyses in which all parasitic mass is distributed such that each perimeter node has either 1/2, 2/3, or 1 times the mass of each interior node; a fourth curve is shown with all the parasitic mass distributed in the same proportion as the structural mass (eq. (10)). The curve for which the perimeter-node parasitic mass to interior-node parasitic mass ratio is 2/3 closely approximates the 3-ring truss frequency data that were computed for exact parasitic mass distributions. As shown in figure 18, a perimeter-node parasitic mass to interior-node parasitic mass ratio of 2/3 closely approximates the actual distribution of truss joint mass for trusses with up to 10 rings. Therefore, the parametric analyses in this report are performed with the assumption that all types of parasitic mass are distributed according to a perimeter-node parasitic mass to interior-node parasitic mass ratio of 2/3.

References

1. Task Committee on Latticed Structures of the Committee on Special Structures of the Committee on Metals of the Structural Division: Latticed Structures: State-of-the-Art Report. *J. Struct. Div.*, Proc. American Soc. Civ. Eng., vol. 102, no. ST11, Nov. 1976, pp. 2197–2229.

2. Topping, B. H. V.: Shape Optimization of Skeletal Structures: A Review. *J. Struct. Eng.*, vol. 109, no. 8, Aug. 1983, pp. 1933–1951.

3. Bush, Harold G.; Herstrom, Catherine L.; Heard, Walter L., Jr.; Collins, Timothy J.; Fichter, W. B.; Wallsom, Richard E.; and Phelps, James E.: Design and Fabrication of an Erectable Truss for Precision Segmented Reflector Application. *J. Spacecr. & Rockets*, vol. 28, no. 2, Mar.–Apr. 1991, pp. 251–257.

4. Dorsey, John T.; and Mikulas, Martin M., Jr.: Preliminary Design of a Large Tetrahedral Truss/Hexagonal Panel Aerobrake Structural System. AIAA-90-1050, Apr. 1990.

5. Mikulas, Martin M., Jr.; Bush, Harold G.; and Card, Michael F.: *Structural Stiffness, Strength and Dynamic Characteristics of Large Tetrahedral Space Truss Structures.* NASA TM X-74001, 1977.

6. Leissa, Arthur W.: *Vibration of Plates.* NASA SP-160, 1969.

7. Mikulas, Martin M., Jr.; Collins, Timothy J.; and Hedgepeth, John M.: *Preliminary Design Approach for Large High Precision Segmented Reflectors.* NASA TM-102605, 1990.

8. Bush, H. G.; Heard, W. L., Jr.; Walz, J. E.; and Rehder, J. J.: *Deployable and Erectable Concepts for Large Spacecraft.* NASA TM-81904, 1980.

9. Whetstone, W. D.: *EISI-EAL Engineering Analysis Language—Interim Release, EAL/325 User Instructions, Version 325.05.* Eng. Inf. Sys., Inc., Jan. 1990.

10. Phadke, Madhav S.: *Quality Engineering Using Robust Design.* Prentice-Hall, 1989.

11. Stanley, Douglas O.; Unal, Resit; and Joyner, C. R.: Application of Taguchi Methods to Dual Mixture Ratio Propulsion System Optimization for SSTO Vehicles. AIAA-92-0213, Jan. 1992.

12. Mikulas, Martin M., Jr.; Wright, Andrew S., Jr.; Bush, Harold G.; Watson, Judith J.; Dean, Edwin B.; Twigg, Leonard T.; Rhodes, Marvin D.; Cooper, Paul A.; Dorsey, John T.; Lake, Mark S.; Young, John W.; Stein, Peter A.; Housner, Jerrold M.; and Ferebee, Melvin J., Jr.: *Deployable/Erectable Trade Study for Space Station Truss Structures.* NASA TM-87573, 1985.

13. Wolfram, Stephen: *Mathematica™—A System for Doing Mathematics by Computer.* Addison-Wesley Publ. Co., Inc., 1988.

Table 1. Empirical Coefficients for Natural Frequency of 1- to 10-Ring Uniform Trusses

n	$f_{\text{unif},0}$, Hz	κ	β	α
1	142.16	0.5610	0.1886	1.8950
2	106.32	.6993	−.0906	−1.3636
3	62.66	.5770	−.1403	−.5139
4	40.95	.4848	−.1647	−.2775
5	28.69	.4152	−.1772	−.1742
6	21.14	.3616	−.1855	−.1175
7	16.19	.3194	−.1907	−.0836
8	12.77	.2856	−.1943	−.0617
9	10.32	.2581	−.1963	−.0469
10	8.51	.2351	−.1974	−.0364

Table 2. Normalized Member Areas and Frequencies for Near-Optimal Trusses With $M_p = 0$ and $\overline{A}_{\max} = 25$

Truss member group	$\overline{A}$ for—					
	$n = 3$	$n = 4$	$n = 5$	$n = 6$	$n = 7$	$n = 8$
1	25.00	25.00	25.00	25.00	25.00	22.96
2	18.03	25.00	11.71	14.30	11.70	13.00
3	25.00	25.00	22.07	15.92	13.68	13.90
4	4.04	24.75	25.00	25.00	25.00	25.00
5	10.50	25.00	12.45	14.30	11.70	13.00
6	19.70	25.00	25.00	25.00	25.00	25.00
7	1.00	1.55	7.74	24.74	25.00	25.00
8	1.00	2.85	14.60	14.30	11.70	13.00
9	1.00	4.86	25.00	25.00	25.00	25.00
10		1.00	1.00	3.79	24.21	25.00
11		1.00	1.00	7.03	11.51	12.98
12		1.00	1.00	11.60	25.00	25.00
13			1.00	1.00	1.65	6.01
14			1.00	1.00	3.53	12.39
15			1.00	1.00	5.50	24.72
16				1.00	1.00	1.52
17				1.00	1.00	1.34
18				1.00	1.00	2.00
19					1.00	1.00
20					1.00	1.00
21					1.00	1.00
22						1.00
23						1.00
24						1.00
$\overline{f}_{\text{opt},0}$	1.83	1.93	1.96	2.02	2.02	2.07

Table 3. Trends in Predicted and Computed $\overline{A}_{max}$ for Near-Optimal 3-Ring Truss Configurations

Parasitic mass fraction	$\overline{A}_{max}$, for—		
	Estimated (fig. 9)	Computed from finite element analysis	
		Node and joint mass	Node, joint, and panel mass
0.25	15	25	
.50	5	14	11
.75	5		9

Table 4. Performance of Near-Optimal Truss Configurations ($\overline{A}_{max} = 5$) With Limited Number of Member Areas and With Joint Stiffness Knockdown

Case	$\overline{A}$ for truss member group—									Limited number of member areas		With joint stiffness knockdown	
	1	2	3	4	5	6	7	8	9	M_p/M_t	$\overline{f}_{opt}$	$\overline{f}_{opt}$	Percent reduction
No parasitic mass:													
3 member areas	5	5	5	3	1	5	1	1	3	0	1.25	1.10	12.00
5 member areas	5	5	5	4	3	5	1	2	2	0	1.32	1.10	16.67
Node and joint parasitic mass:													
3 member areas	5	5	5	5	3	5	1	3	5	0.44	0.81	0.66	18.52
5 member areas	5	5	5	5	4	5	1	3	4	.44	.82	.66	19.51
Node, joint, and panel parasitic mass:													
3 member areas	5	5	5	5	5	5	1	5	5	0.72	0.51	0.41	19.61
5 member areas	5	5	5	5	5	5	2	5	5	.72	.52	.41	21.15

Table 5. Empirical Coefficients for 1- to 10-Ring Uniform Trusses

n	d, m	$f_{unif,0}$, Hz	κ	$M_p/M_t\|_{\delta=\delta_{max}}$	δ_{max}	β	α
1	6	142.160	0.5610	0.5999	0.1203	0.1886	1.8950
2	10	106.321	.6993	.6494	.0476	−.0906	−1.3636
3	14	62.658	.5770	.6596	.0286	−.1403	−.5139
4	18	40.945	.4848	.6647	.0183	−.1647	−.2775
5	22	28.690	.4152	.6674	.0125	−.1772	−.1742
6	26	21.142	.3616	.6691	.0089	−.1855	−.1175
7	30	16.188	.3194	.6703	.0065	−.1907	−.0836
8	34	12.772	.2856	.6711	.0049	−.1943	−.0617
9	38	10.324	.2581	.6715	.0038	−.1963	−.0469
10	42	8.511	.2351	.6718	.0029	−.1974	−.0364

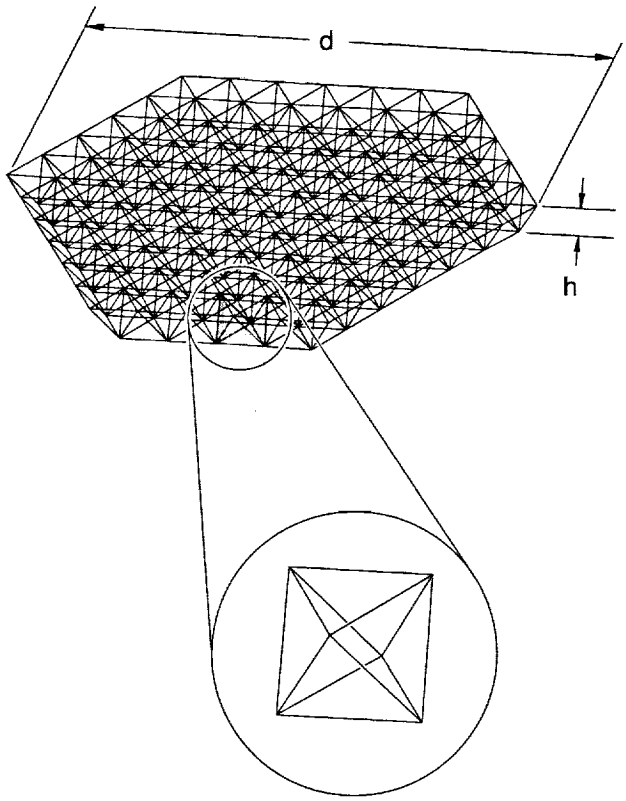

(a) With unit cell.

Figure 1. Tetrahedral truss platform.

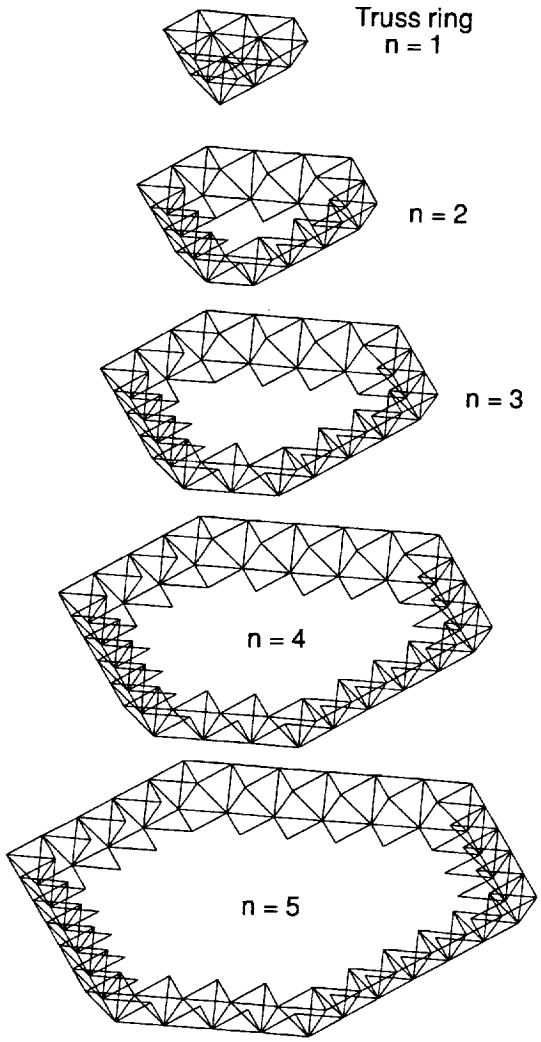

(b) Subdivided into truss rings.

Figure 1. Continued.

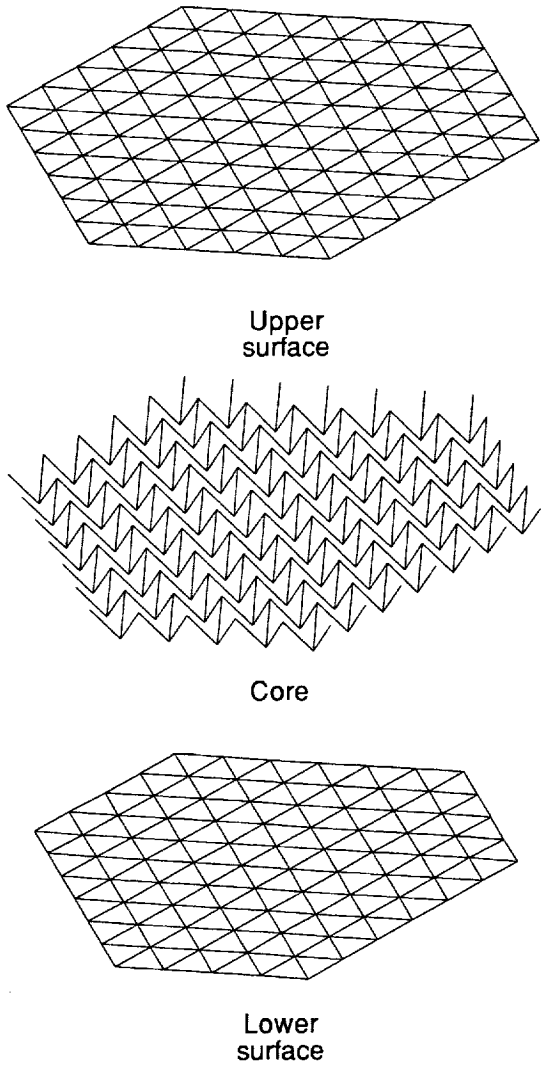

(c) Subdivided into upper surface, core, and lower surface.

Figure 1. Concluded.

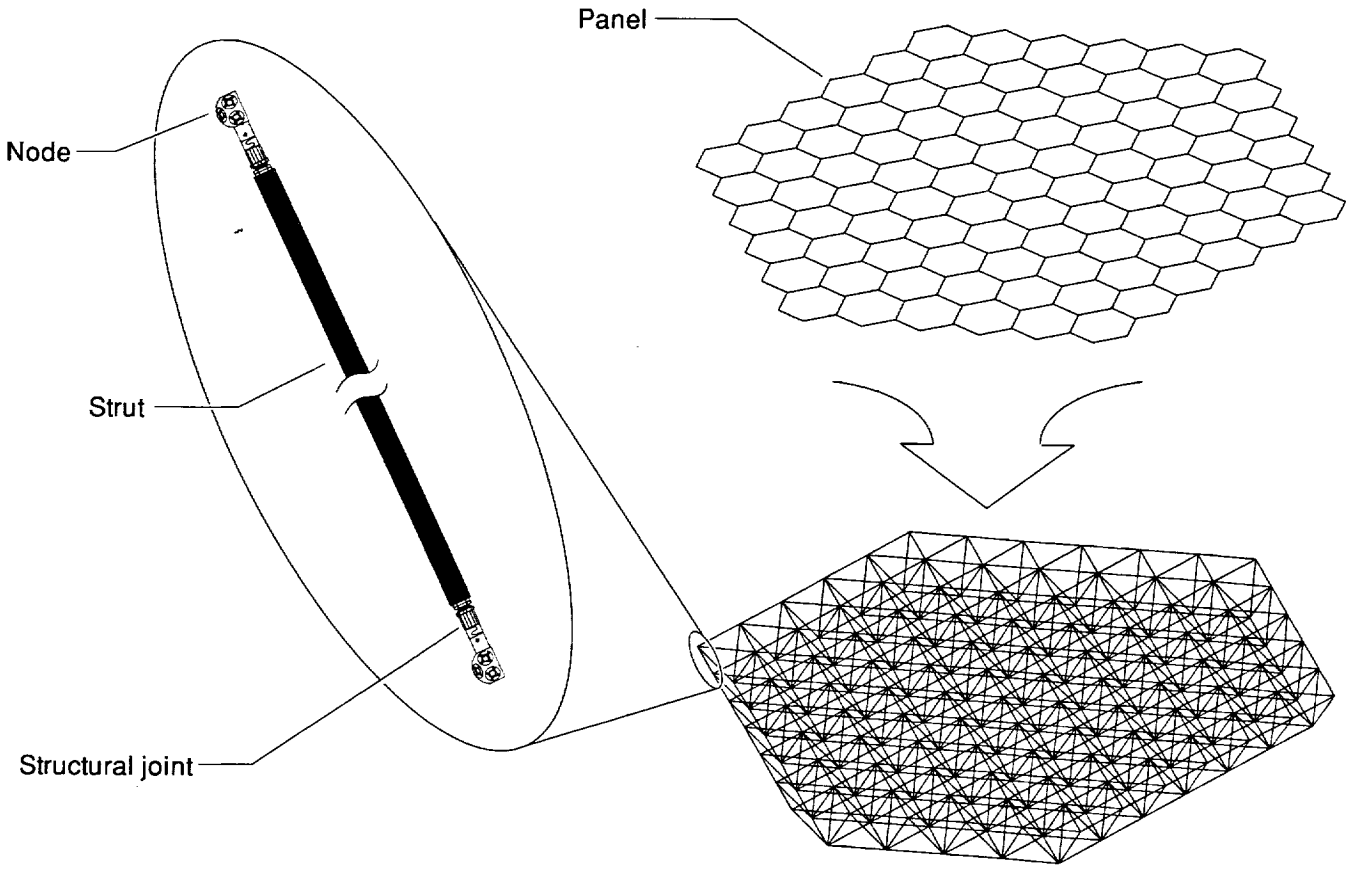

(a) Truss-member detail.

(b) Hexagonal panel array.

Figure 2. Tetrahedral truss platform details.

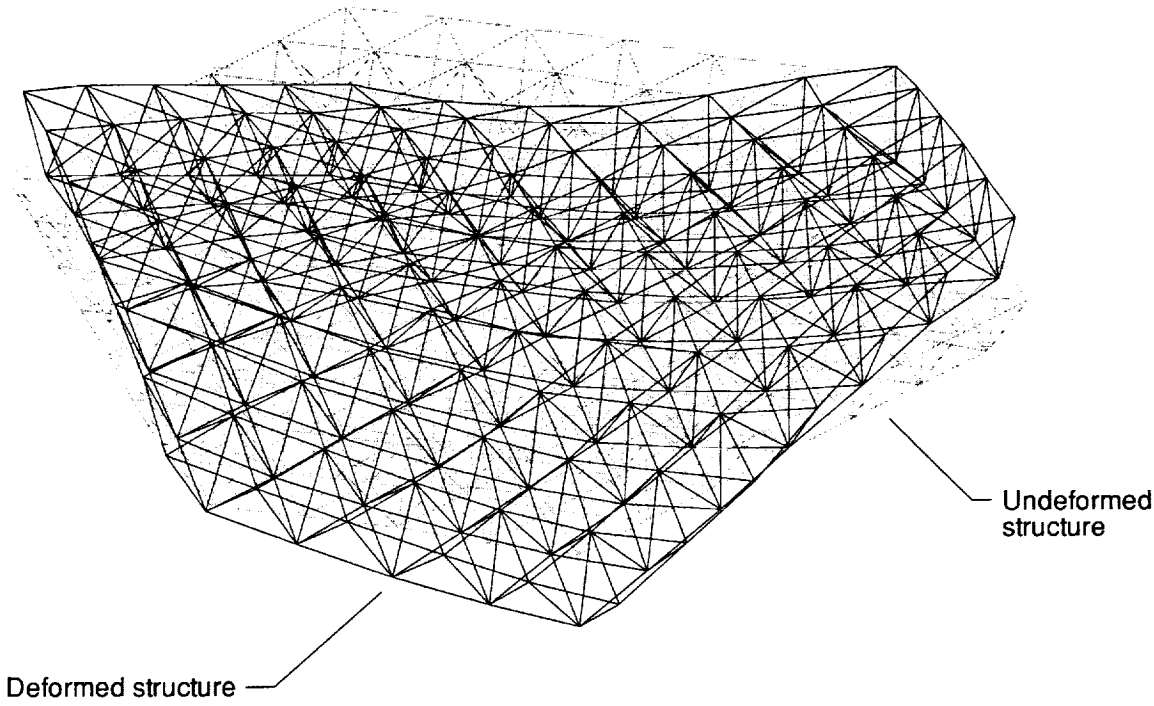

Figure 3. Mode shape for fundamental mode of free-free 5-ring truss platform.

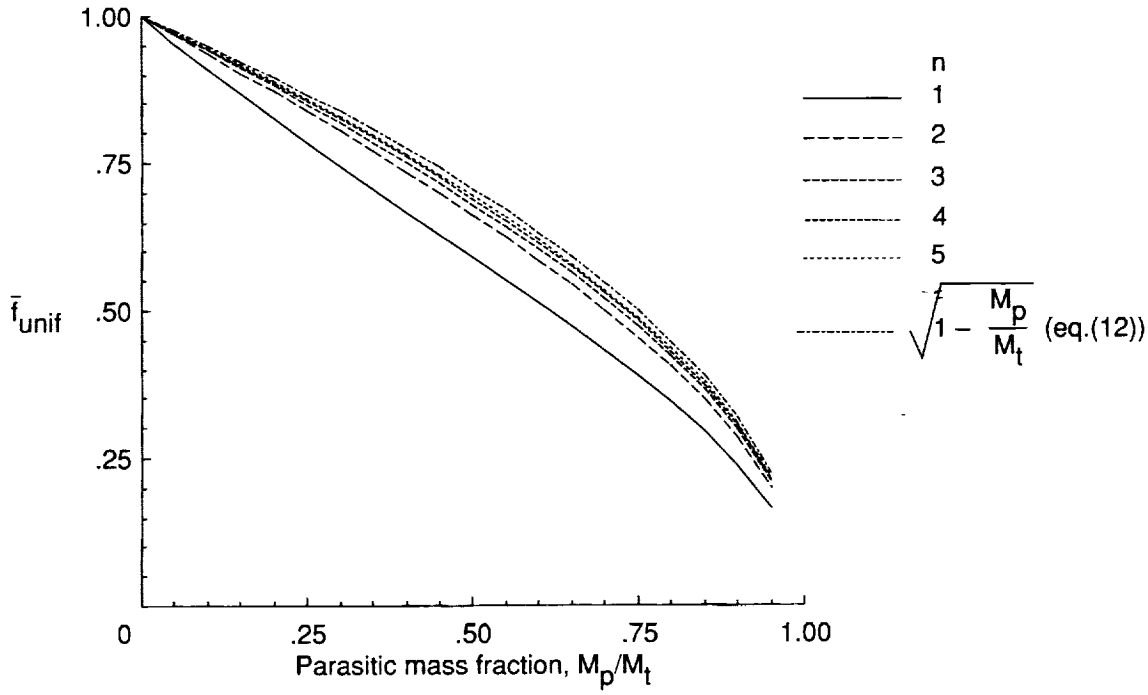

Figure 4. Normalized frequency for 1- to 5-ring uniform trusses.

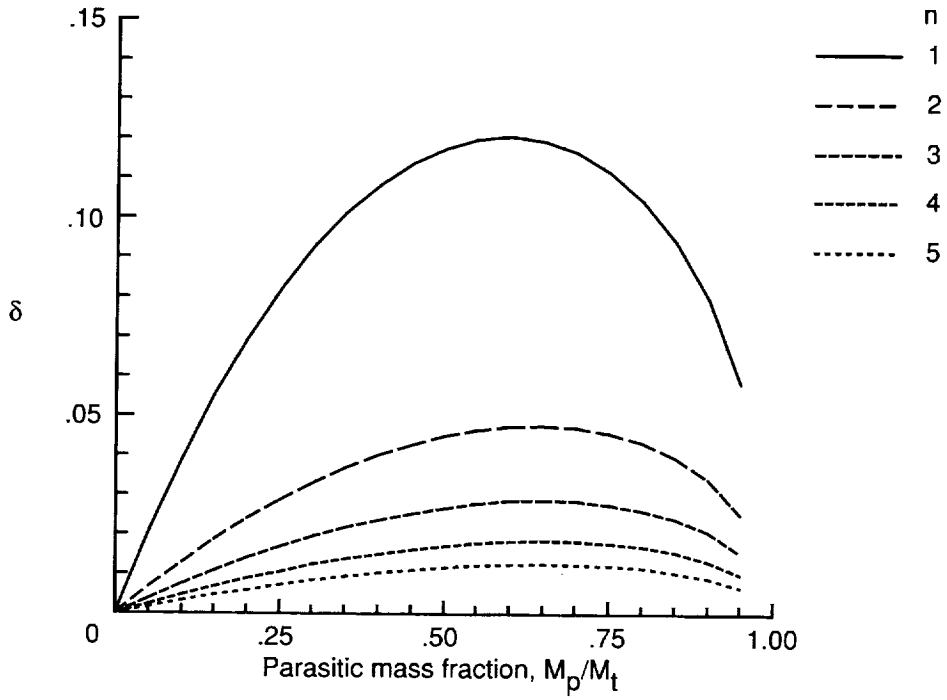

Figure 5. Correction term δ for 1- to 5-ring uniform trusses.

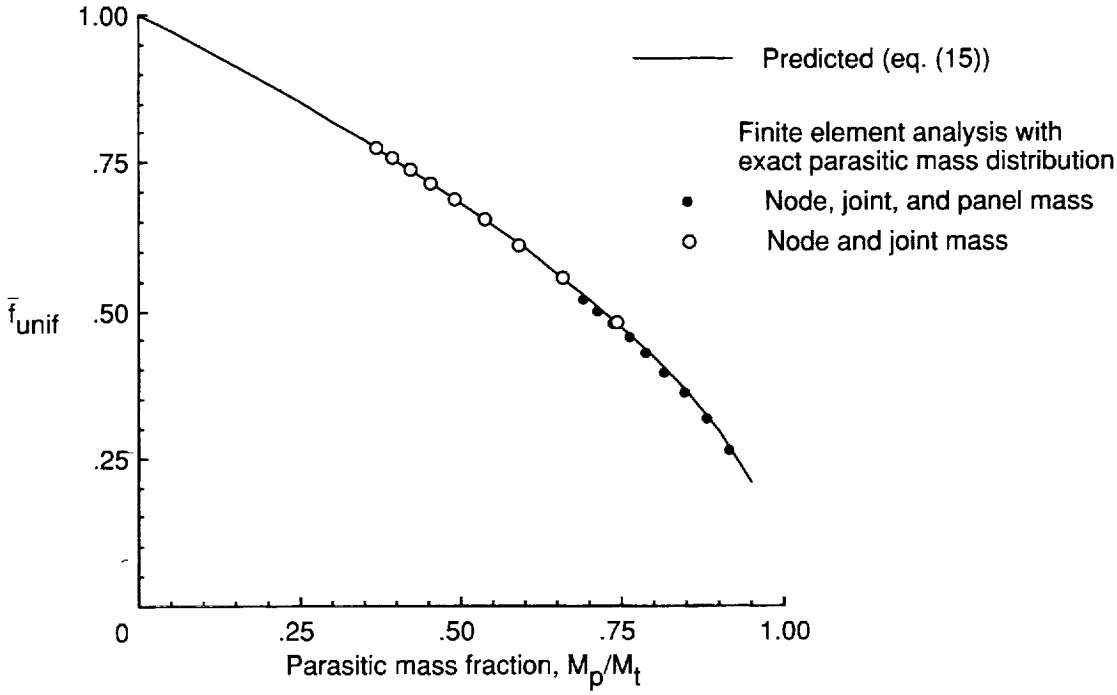

(a) 3-ring truss.

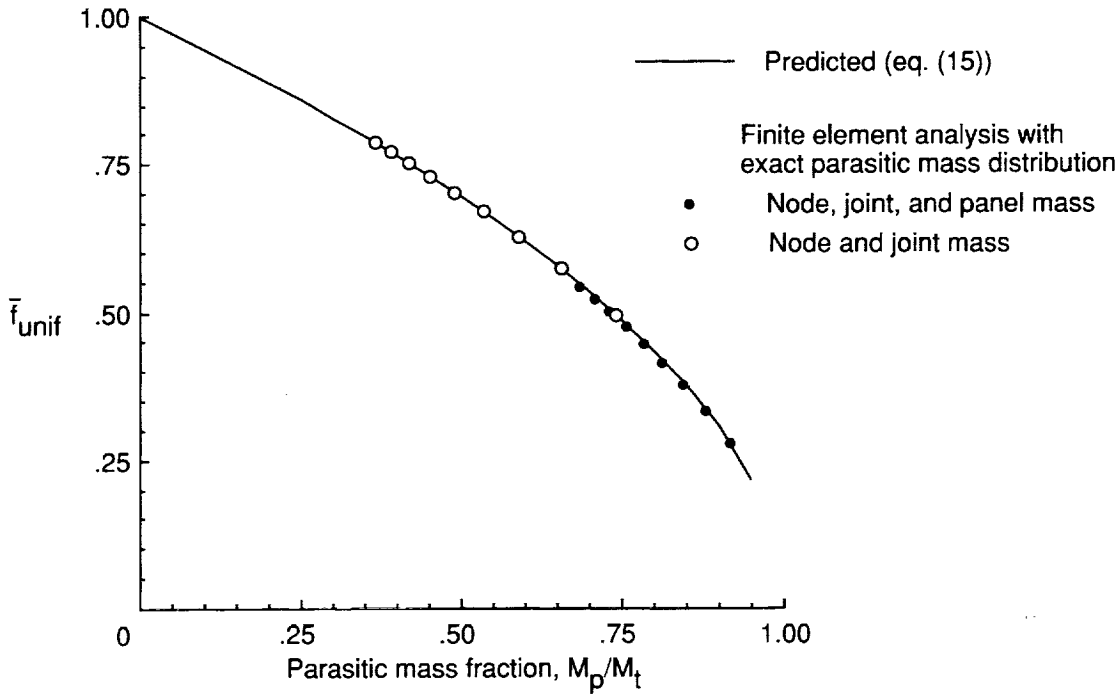

(b) 5-ring truss.

Figure 6. Predicted and computed normalized frequencies of uniform trusses.

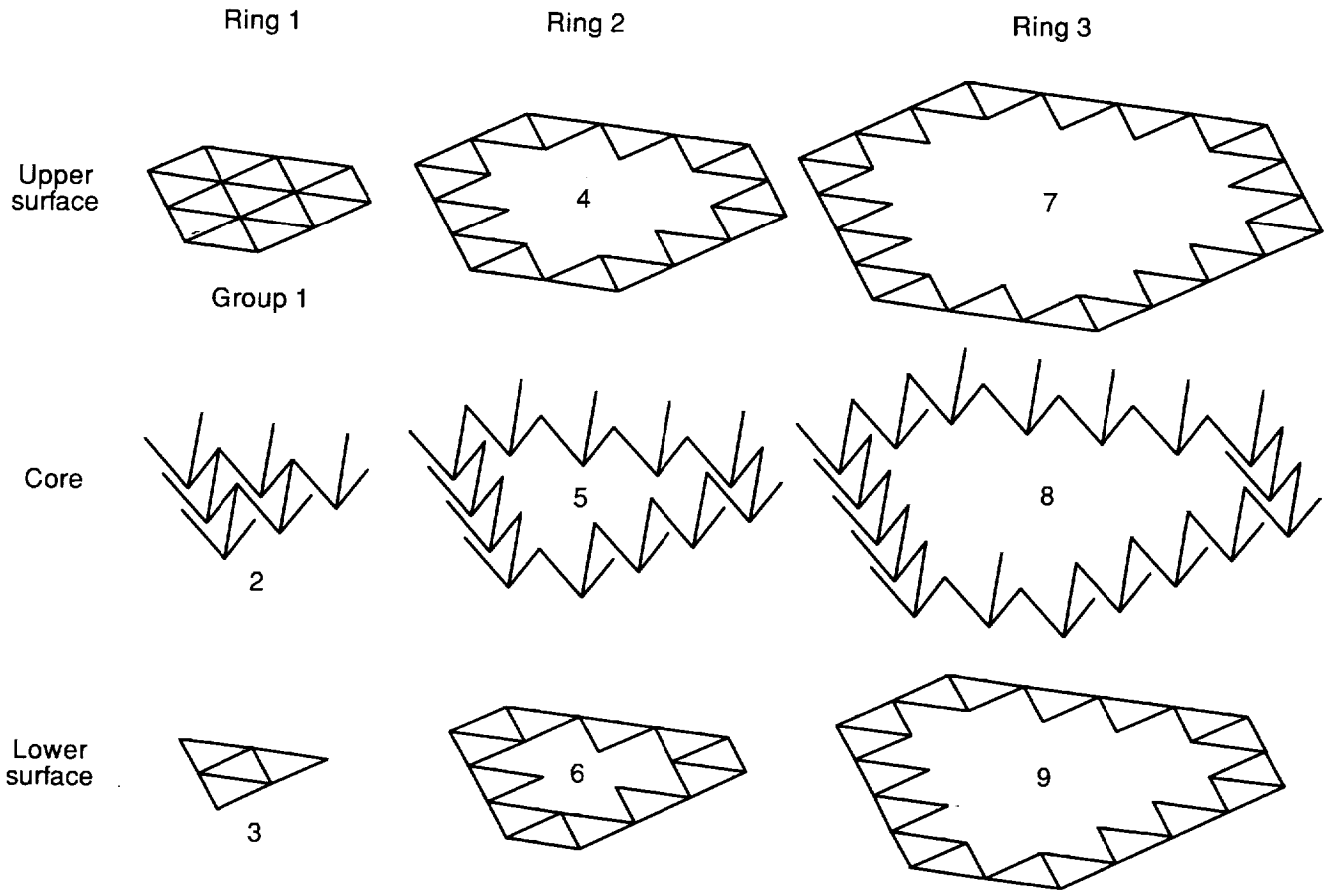

Figure 7. Member groups (1 to 9) for a 3-ring truss.

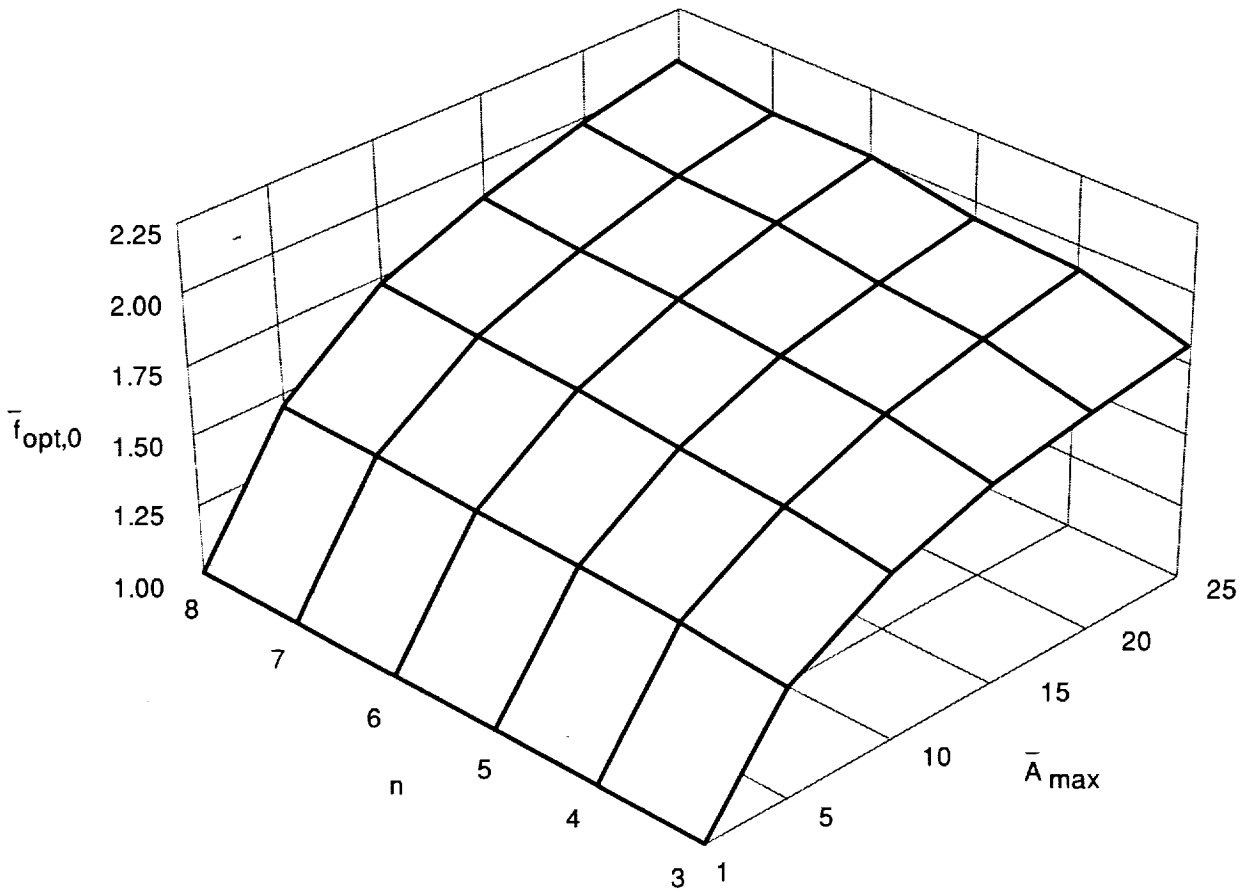

Figure 8. Near-optimal normalized frequencies for varying n and $\overline{A}_{\max}$ for trusses with no parasitic mass.

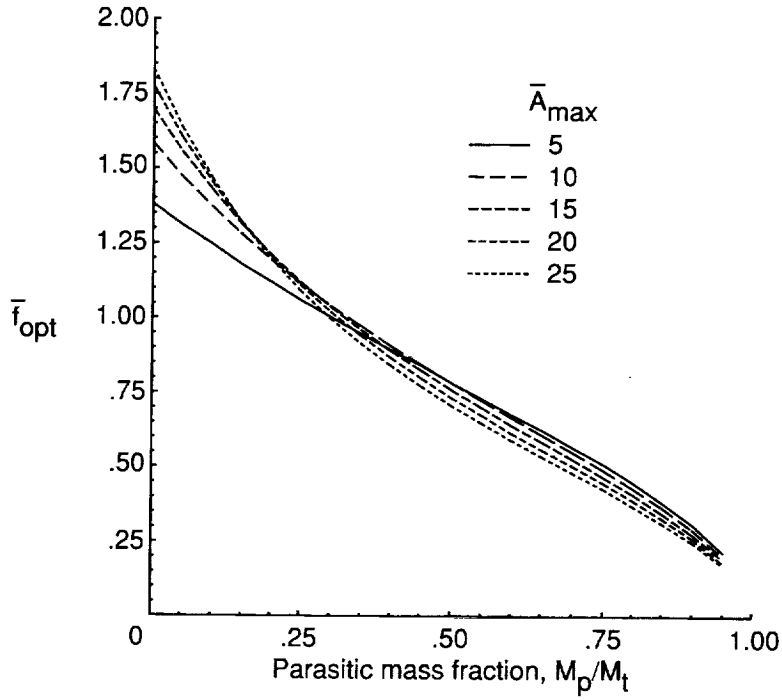

Figure 9. Variation in 3-ring truss normalized frequencies for ranges of $\overline{A}_{\max}$ and M_p/M_t.

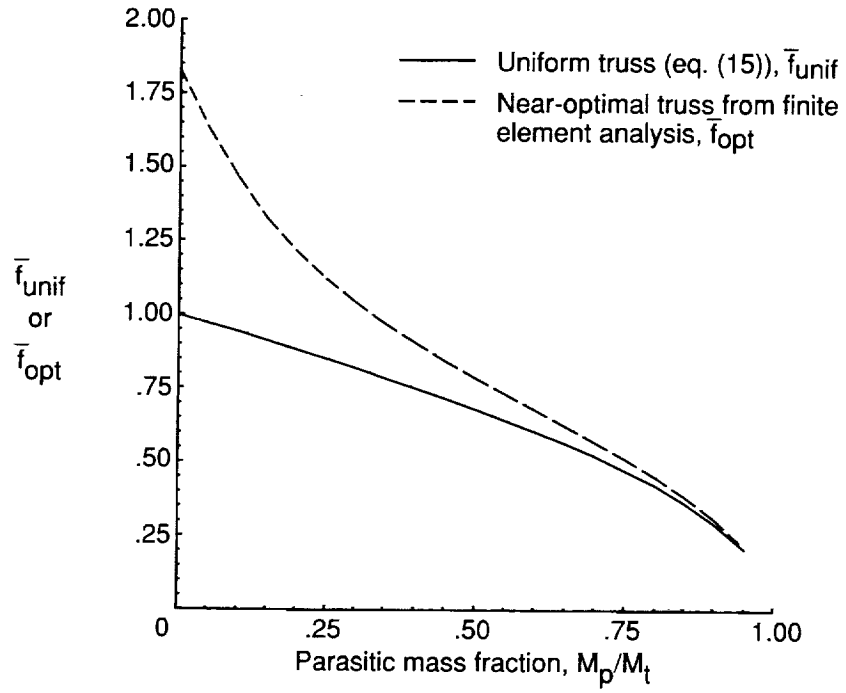

Figure 10. Normalized frequency of 3-ring uniform and near-optimal trusses.

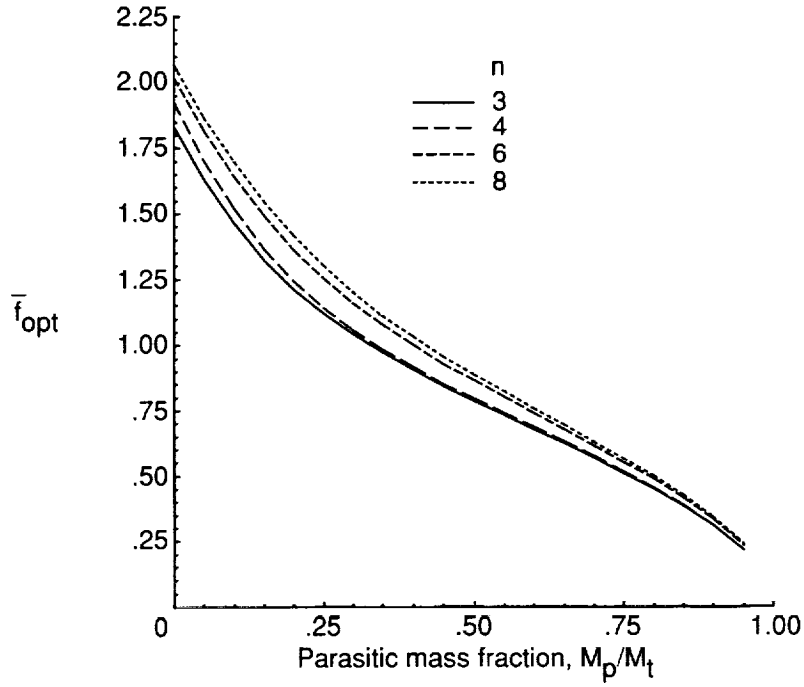

Figure 11. Normalized frequency of 3- to 8-ring near-optimal trusses.

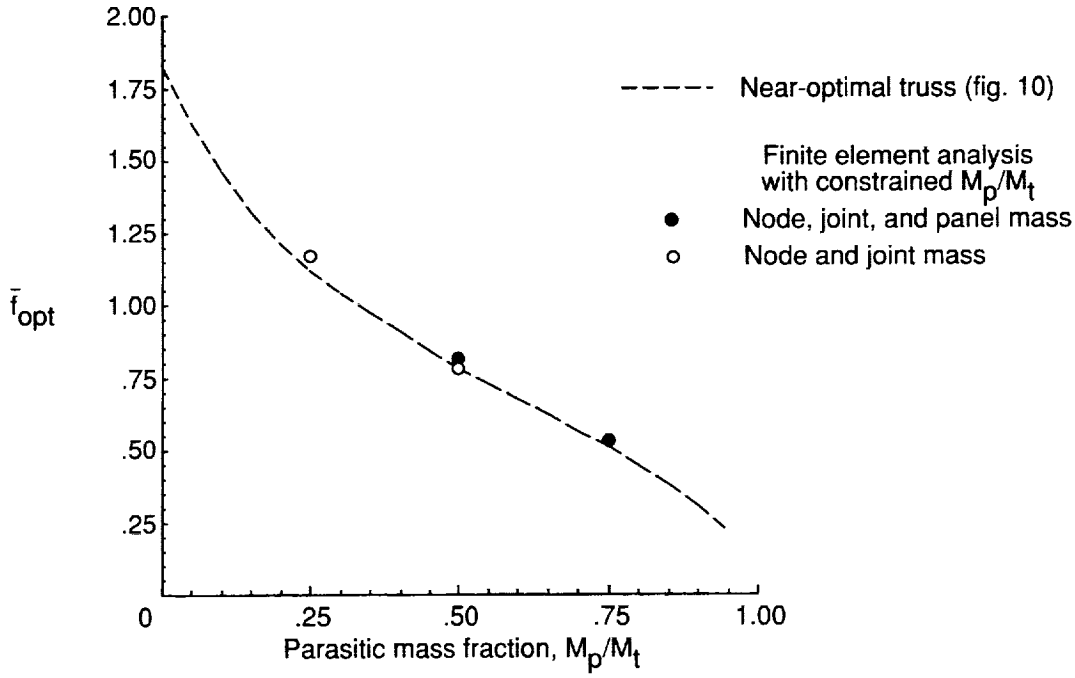

Figure 12. Predicted and computed normalized frequencies of 3-ring near-optimal trusses.

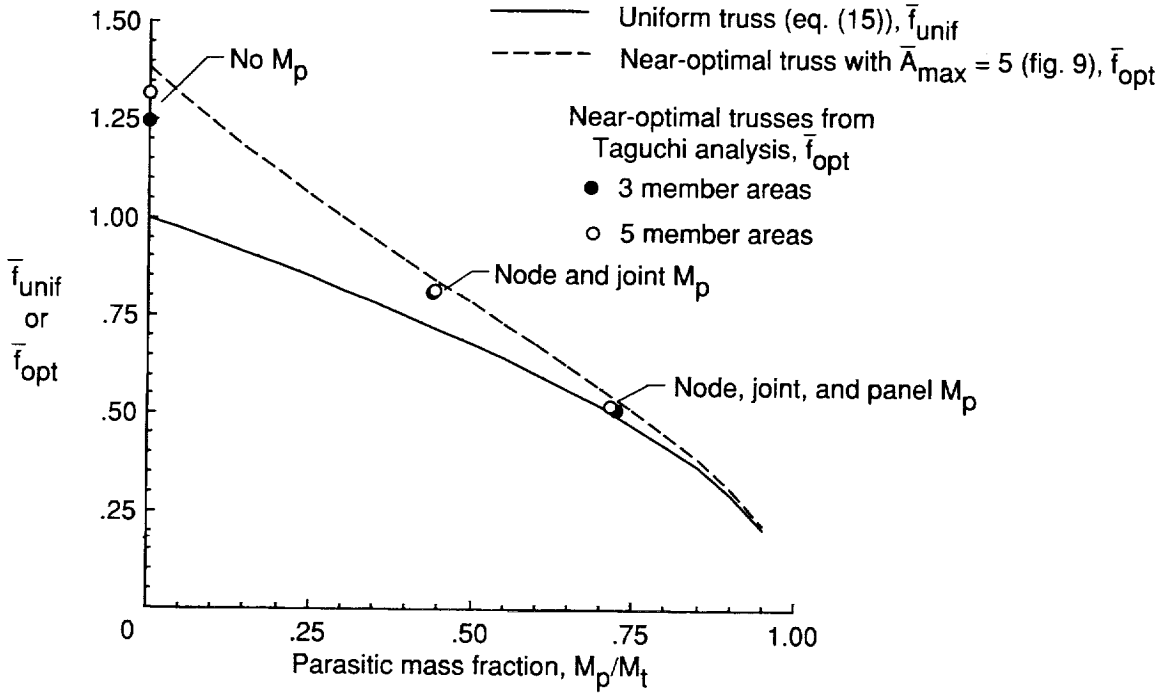

Figure 13. Normalized frequency of 3-ring truss with limited number of member areas.

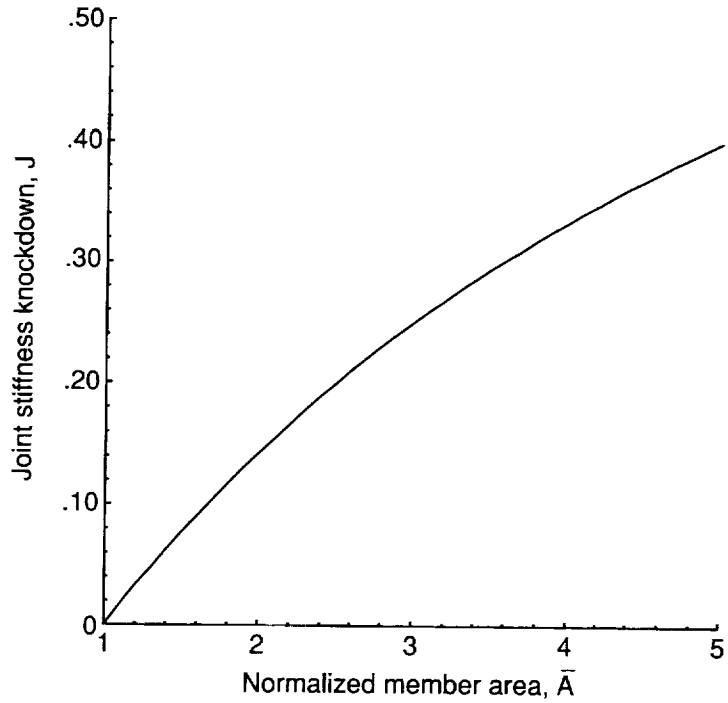

Figure 14. Variation in joint stiffness knockdown with normalized member area.

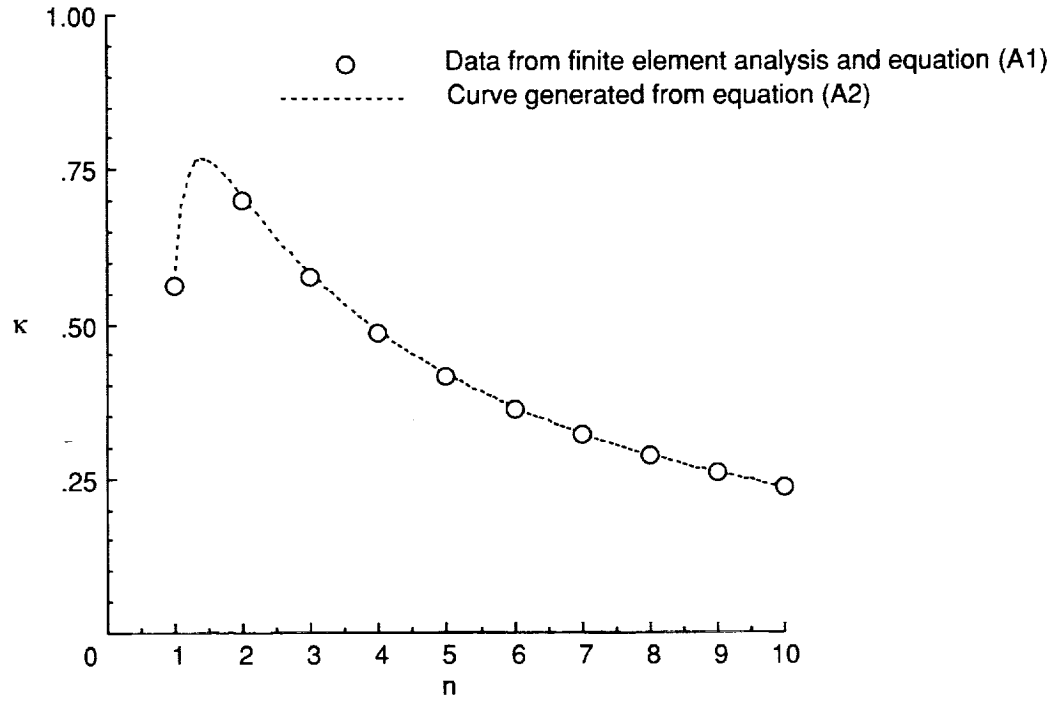

Figure 15. Variation of coefficient κ with truss n.

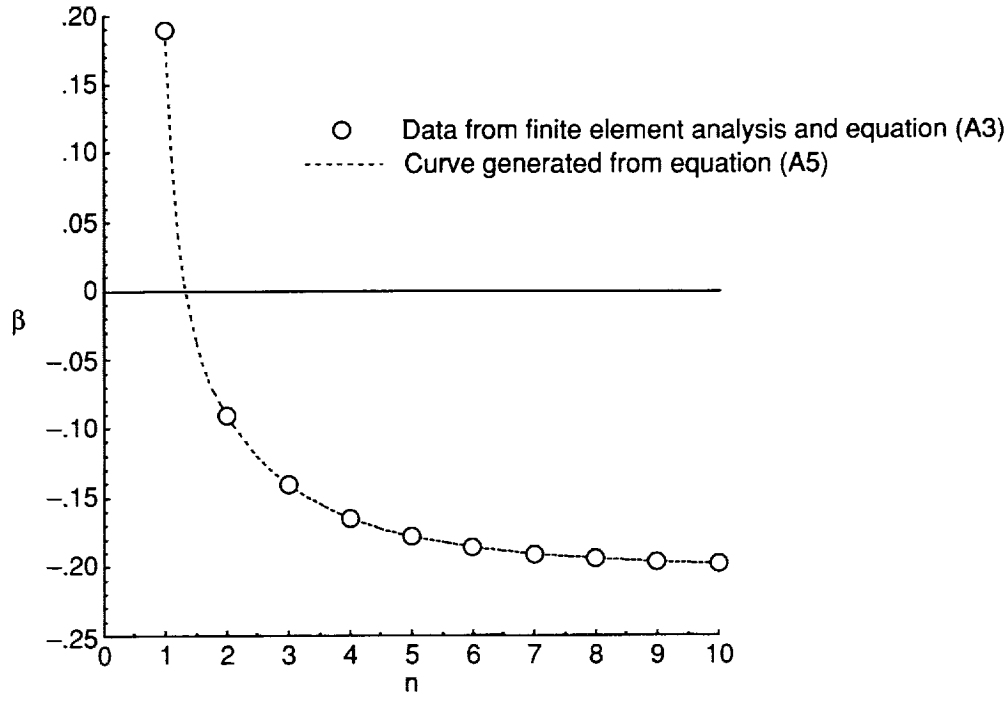

Figure 16. Variation of coefficient β with truss n.

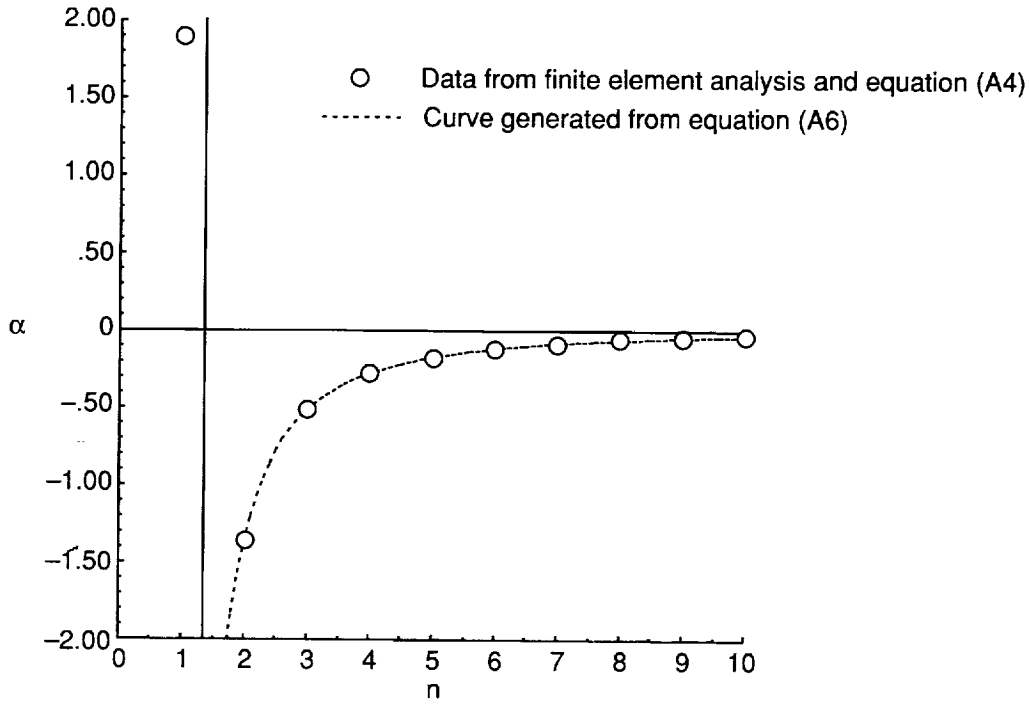

Figure 17. Variation of coefficient α with truss n.

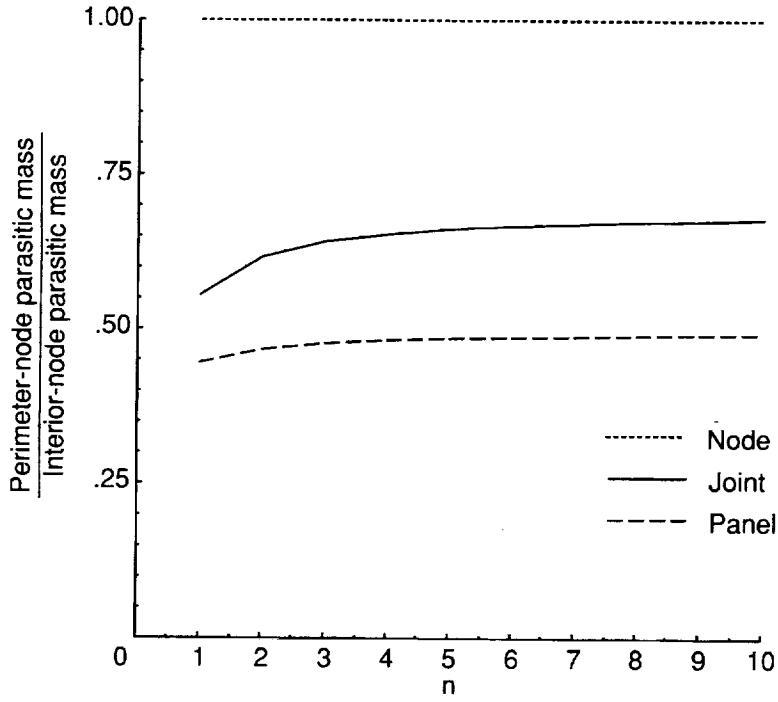

Figure 18. Ratio of perimeter-node parasitic mass to interior-node parasitic mass for nodes, joints, and panels.

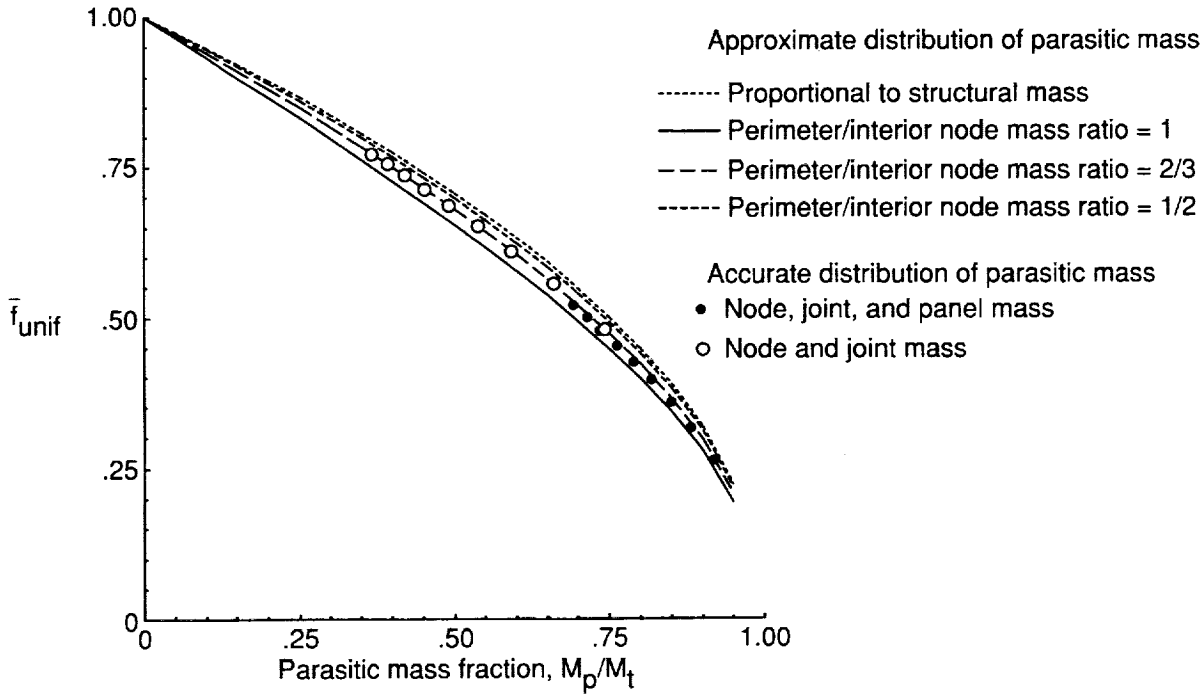

Figure 19. Normalized frequencies of 3-ring truss for various parasitic mass distributions.

REPORT DOCUMENTATION PAGE

Form Approved
OMB No. 0704-0188

1. AGENCY USE ONLY *(Leave blank)*	2. REPORT DATE	3. REPORT TYPE AND DATES COVERED
	November 1994	Technical Paper

4. TITLE AND SUBTITLE
Natural Frequency of Uniform and Optimized Tetrahedral Truss Platforms

5. FUNDING NUMBERS
WU 506-43-41-02

6. AUTHOR(S)
K. Chauncey Wu and Mark S. Lake

7. PERFORMING ORGANIZATION NAME(S) AND ADDRESS(ES)
NASA Langley Research Center
Hampton, VA 23681-0001

8. PERFORMING ORGANIZATION REPORT NUMBER
L-17307

9. SPONSORING/MONITORING AGENCY NAME(S) AND ADDRESS(ES)
National Aeronautics and Space Administration
Washington, DC 20546-0001

10. SPONSORING/MONITORING AGENCY REPORT NUMBER
NASA TP-3461

11. SUPPLEMENTARY NOTES

12a. DISTRIBUTION/AVAILABILITY STATEMENT
Unclassified–Unlimited
Subject Category 18
Availability: NASA CASI (301) 621-0390

12b. DISTRIBUTION CODE

13. ABSTRACT *(Maximum 200 words)*

Qualitative and quantitative estimates for the fundamental frequency of uniform and optimized tetrahedral truss platforms are determined. A semiempirical equation is developed for the frequency of free-free uniform trusses as a function of member material properties, truss dimensions, and parasitic (nonstructural) mass fraction M_p/M_t. Optimized trusses with frequencies approximately two times those of uniform trusses are determined by varying the cross-sectional areas of member groups. Trusses with 3 to 8 rings, no parasitic mass, and member areas up to 25 times the minimum area are optimized. Frequencies computed for ranges of both M_p/M_t and the ratio of maximum area to minimum area are normalized to the frequency of a uniform truss with no parasitic mass. The normalized frequency increases with the number of rings, and both frequency and the ratio of maximum area to minimum area decrease with increasing M_p/M_t. Frequency improvements that are achievable with a limited number of member areas are estimated for a 3-ring truss by using Taguchi methods. Joint stiffness knockdown effects are also considered. Comparison of optimized and baseline uniform truss frequencies indicates that tailoring can significantly increase structural frequency; maximum gains occur for trusses with low values of M_p/M_t. This study examines frequency trends for ranges of structural parameters and may be used as a preliminary design guide.

14. SUBJECT TERMS	15. NUMBER OF PAGES
Natural frequency; Optimization; Space structures; Taguchi methods; Truss design	31
	16. PRICE CODE A03

17. SECURITY CLASSIFICATION OF REPORT	18. SECURITY CLASSIFICATION OF THIS PAGE	19. SECURITY CLASSIFICATION OF ABSTRACT	20. LIMITATION OF ABSTRACT
Unclassified	Unclassified	Unclassified	